Marshall University
Marshall Digital Scholar

Theses, Dissertations and Capstones

1996

Modulated structures in electrodeposited superconducting Ba(1-x)K(x)BiO(3)

Chad Bryant Huffman

Follow this and additional works at: https://mds.marshall.edu/etd

Part of the Biochemistry Commons, Cell and Developmental Biology Commons, and the Molecular Biology Commons

MODULATED STRUCTURES IN ELECTRODEPOSITED SUPERCONDUCTING $Ba_{1-x}K_xBiO_3$

A Thesis Presented to the Department of Chemistry at Marshall University in Partial Fulfillment of the Requirements for the Degree of Master of Science.

by

Chad Bryant Huffman

Marshall University

June, 1996

Marshall University

Department of Chemistry

This thesis was accepted on June 24, 1996

as meeting the research requirements for the degree of Master of Science.

Advisor, Department of Chemistry

Member, Department of Chemistry

Member, Department of Chemistry

Dean, Graduate School

This work is dedicated to my parents.

Their immense support and confidence have enriched my life and happiness. I thank them for everything I have and am.

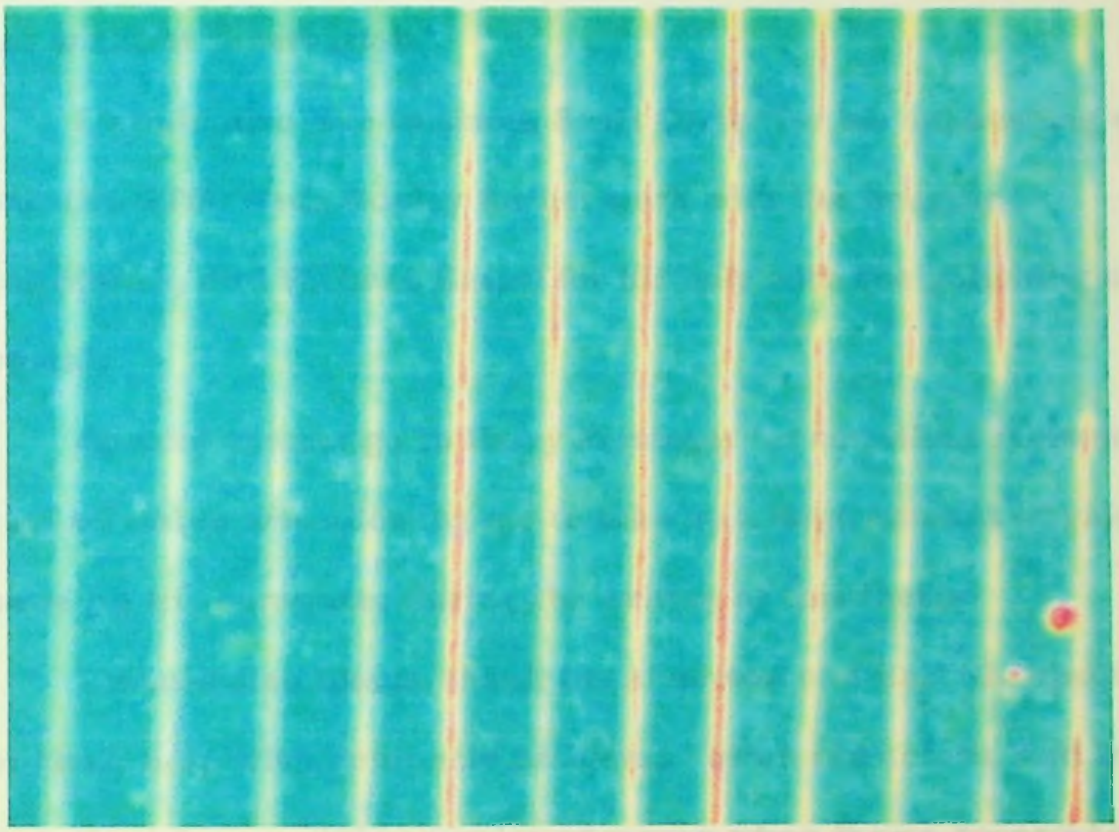

Acknowledgments

Throughout this work, Dr. Norton has supported my efforts. He has provided advice, direction and support on a legion of occasions. He has an enormous facility for giving guidance, and has an even greater reserve of patience. For these reasons, I would like to thank him without reservation.

I would also like to thank Scott Carter for his exhausting work with the STM. Veda Copley for her work with the imaging techniques, and Richard Kassel for his help with the polishing of the crystals.

Special thanks go to Harry Persinger for countless reasons, the least of which was allowing me to take up a large amount of valuable space on his computer during the writing of this thesis.

I would also like to thank Dr. Anderson and Karl Shanholtzer for their help with computer problems I often ran across, and Dr. Castellani for providing a voice of reason when it was desperately needed.

Furthermore, thanks go out to all of the chemistry faculty and staff for all their help during my studies at Marshall University. I definitely needed it. I couldn't have gotten through without their help.

Abstract 1
Introduction : Superconductors, Multilayer Systems, and
Electrodepositing Superconductors 2
Superconductivity 2
Multilayers 5
Electrodeposition of $Ba_{1-x}K_xBiO_3$ (BKBO) 6
Potential - Compositional Relationship in the
$(Ba,K)BiO_3$ System 7
Electrodeposition of $Ba_{1-y}K_yBi_{1-x}Pb_xO_3$ (BKPBO) 10
Potential - Compositional Relationship in the
$(Ba,K)(Bi,Pb)O_3$ System 10
Project Objective 12
Materials and Methods 13
Electrochemical Equipment 13
Chemicals Used and Molar Ratios in Solution 15
Electrodeposition Procedure 16
Depositing Modulated Materials 20
Harvesting Crystals 20
Crystal Polishing Procedure 22
Mounting Crystals in Bakelite Rings 25
Grinding and Polishing the Epoxied Crystals 28
Microscopy and Images 29
Results and discussion 30
Optical Imaging 30
$(Ba,K)(Bi,Pb)O_3$ 30
$(Ba,K)BiO_3$ 34
STM Imaging 39
Comparison of STM and Optical Images 43
SEM Backscattered Electron Imaging and
Etching the Surface of the Crystal 46

Growth Rate Measurements 48
Temporal Dependence of Current 51
Current Spikes Accompanying a Potential Transition..... 53
Superconductivity of Modulated Structure 57
Conclusion 59
References 61

List of Tables

Table 1; Chemicals Used 15
Table 2; Width of Modulated Layers as a Function of Time 48

List of Figures

Figure 1; Pairing of electrons in superconducting lattice 3
Figure 2; BKBO unit cell 6
Figure 3; Potassium content *vs.* overpotential for BKBO 8
Figure 4; T_c *vs.* Potassium content for BKBO 9
Figure 5; Composition of BKPBO *vs.* potential 10
Figure 6; T_c *vs.* total dopant concentration for BKPBO 11
Figure 7; Block diagram of electronic equipment used 14
Figure 8; Teflon holder for large cell 18
Figure 9; Details of cell 19
Figure 10; Direction of crystal growth 22
Figure 11; Idealized cut crystal 23
Figure 12; Effect of orientation on appearance of cross section ... 24
Figure 13; Slide taped to counter top 26
Figure 14; Optical image of multilayered BKPBO 33
Figure 15; Image of multilayered BKBO 34
Figure 16; Gray Scale of BKBO grown with equal times 35

Figure 17; Gray scale of image used for optical intensity 36
Figure 18; Vertical optical intensity 37
Figure 19; Horizontal optical intensity 37
Figure 20; STM image of layered crystal 40
Figure 21; Cross section of Figure 20 40
Figure 22; Gray Scale of STM image 43
Figure 23; Gray scale of optical image of crystal imaged by STM .. 44
Figure 24; Backscattered SEM image of an untreated crystal 46
Figure 25; Backscattered SEM image of a treated crystal 46
Figure 26; Red layer thickness *vs.* cycle time 49
Figure 27; Blue layer thickness *vs.* cycle time 49
Figure 28; Typical current plots
for nonmodulated and modulated growth 51
Figure 29; Potential program 53
Figure 30; Plot of current transitions 54
Figure 31; Current transition accompanying potential
switch from 0.68 V to 0.66 V 55
Figure 32; Current transition accompanying potential
switch from 0.66 V to 0.68 V 56
Figure 33; Magnetic susceptibility of growth #4 58

Abstract

Compositionally modulated crystals of the superconductor $Ba_{1-x}K_xBiO_3$ have been grown electrochemically. Modulation was produced through control of the deposition potential.

Modulated crystals were imaged using optical microscopy, backscattered SEM, and STM. The expected linear relationship between the amount of time that current was applied and the modulation thickness was observed, and the growth rates were determined.

Multilayers were differentially etched using an EDTA solution. Etched and unetched samples were imaged using backscattered SEM.

The transition temperature of a modulated sample was determined by SQUID magnetometry to equal the bulk value.

Introduction : Superconductors, Multilayer Systems, and Electrodepositing Superconductors

Superconductivity

In 1911, the Dutch physicist, Kamerlingh-Onnes, was conducting experiments on the resistance of mercury at low temperatures. As he cooled a sample in liquid helium, he observed the resistance drop to zero. This was a sharp discontinuity which did not follow the trend that he observed at higher temperatures. He named this state "superconducting". Soon after, other elements were found to be superconducting at sufficiently low temperatures (1). Niobium, with a superconducting temperature of 9 K, has the highest superconducting temperature of the elements (2).

One of the most successful theories attempting to explain superconductivity was set forth by Bardeen, Cooper and Schrieffer in 1957, often referred to as the BCS theory. Electrons are mutually repulsive, but in this theory electrons are paired as they move through the solid as diagrammed in Figure 1. The energy that one electron loses to the surrounding lattice is gained by the other through an interaction with lattice vibrations called phonons. A pair of electrons moving through a lattice is called a Cooper pair (3).

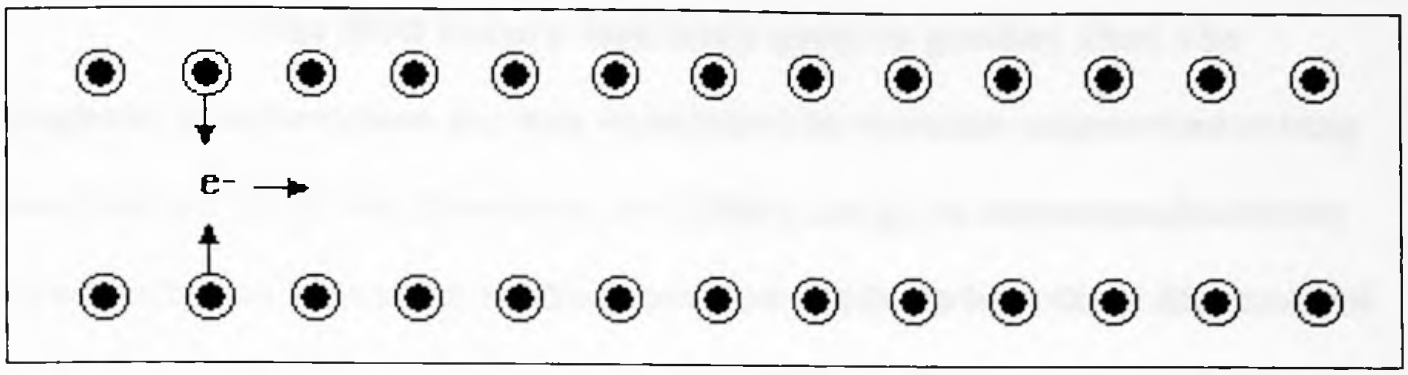

Fig. 1a, As an electron travels through a crystal it attracts the positive ions of the lattice toward it.

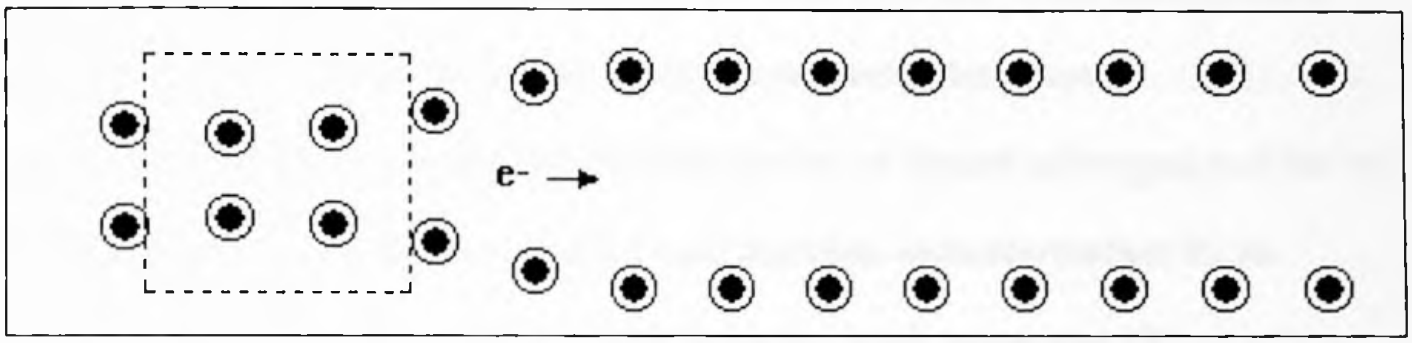

Fig. 1b, The electron continues through the lattice, leaving in its wake an area of electropositive charge. This is indicated by the dashed box above.

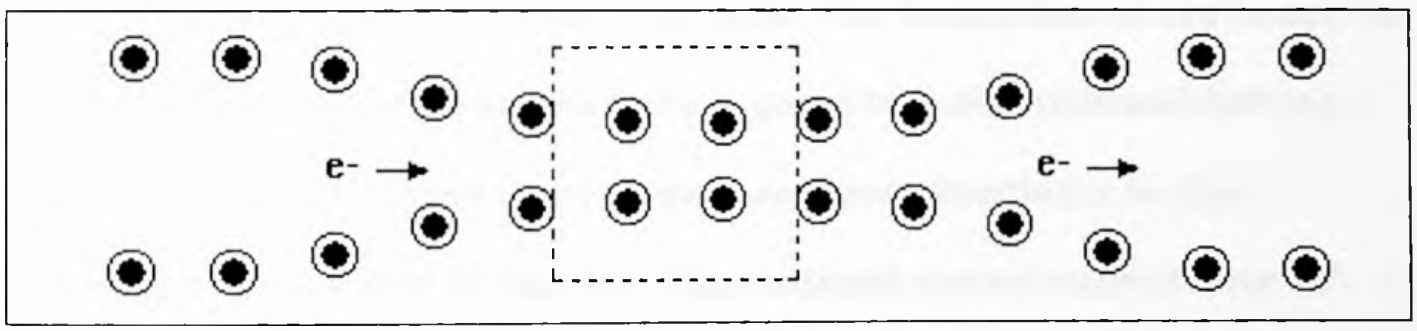

Fig. 1c, A second electron can be attracted by the electropositive area. In this way the electrons are effectively paired through an induced lattice vibration or a phonon.

Fig. 1, Pairing of electrons in a superconducting crystal lattice.

The BCS theory had been used to predict that the highest temperature for any substance to become superconducting was about 25 K (4). However, in 1986 a surge in superconductivity research was initiated by Bednorz and Müller when they discovered a high temperature superconductor (HTSC). This compound was a cuprate with a superconducting temperature of 30 K (5). In March of 1987 $YBa_2Cu_3O_7$ was reported by Wu and Chu (6). This compound had a T_c (the temperature at which a material becomes superconducting) above the boiling point of liquid nitrogen (-196 °C, 77 K). So far, the material with the highest substantiated T_c is $HgBa_2Ca_2Cu_3O_x$ with a T_c of 164 K under high pressure (7).

Although the cuprates currently hold the highest T_c, a second class of HTSC (the bismuthates) was discovered earlier (8) which differs considerably from the cuprates. The bismuthates are cubic in structure while the cuprates have a quasi two-dimensional lattice. This provides for three dimensional superconductivity in the bismuthates instead of the two dimensional superconductivity of the cuprates (9,10). Also, $Ba_{0.6}K_{0.4}BiO_3$ has a larger coherence length than that of the cuprates, about 60 Å for the bismuthates and about 3 Å for the cuprates (11).

MULTILAYERS

Multilayers were first studied in the mid 1930's by DuMond and Yortz. They produced a multilayer of gold and copper in thin films. This was then used as a diffraction grating for soft x-rays (12). In 1968, Strongin *et al.* observed increases in the T_c of thin alternating layers of Al and Sn as well as Al and Cu(13).

More recently, a specific type of multilayer has found use in Josephson Junctions. Josephson Junctions consist of an insulating layer separating two superconductive layers. Electrons tunnel from one superconducting layer, through the insulating layer, to the second superconducting layer. These junctions can be arranged to form a Superconducting Quantum Interference Device (SQUID), which is used to detect small changes in magnetic fields (14).

Multilayered superconductors are also of interest as a model system for studying the problems of vortex lines in HTSC's (15). The advantage of producing multilayers as opposed to studying the fixed layer spacing of the copper based superconductors is that the size of the layers can be controlled.

Electrodeposition of $Ba_{1-x}K_xBiO_3$ (BKBO)

All crystals in our experiments were grown in a KOH melt at a temperature of 260 °C. This is comparatively low in temperature relative to other techniques used to make the material. Molecular Beam Epitaxy heats the substrate during deposition, which is followed by annealing in an oxygen enriched atmosphere to create the stoichiometric oxide (16). Ceramic methods use high temperatures as well, and produce polycrystalline materials. In one ceramic technique, temperatures in excess of 700 °C are used (17).

BKBO has a cubic structure with bismuth in the center of the cube, barium at each of the corners and oxygen atoms in the center of each face. Potassium can be substituted in the barium sites (Figure 2) (18).

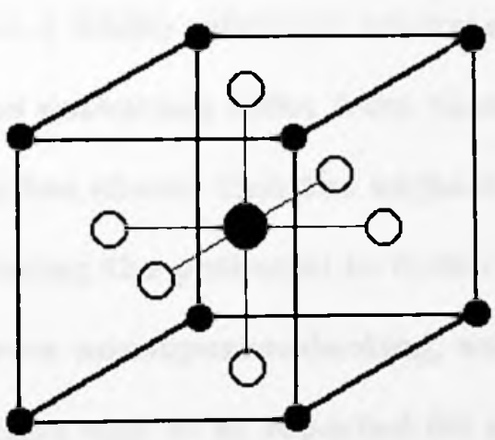

Fig. 2, BKBO unit cell

Single crystals were first grown by electrodeposition by Norton in 1989 using a two electrode cell (19). Norton improved this process in 1991 by the use of a three electrode cell which had a Bismuth reference electrode (20). Since then, a series of crystals with different compositions have been grown using this method (21).

These different compositions, grown under identical conditions with potential as the only variable, have different T_c's. These range from a T_c of 32 K for x = 0.38 to a T_c of 12 K for x = 0.54.

Potential - Compositional Relationship in the (Ba,K)BiO_3 System

Han *et al.* reported the variation of x (potassium concentration) *vs.* overpotential for their growth of crystals of $Ba_{1-x}K_xBiO_3$ (22). Because a BKBO reference electrode was used by Han *et al.*, their reported potentials differ from those used here. Experience in our group has shown that the highest T_c occurs at a potential of 0.68V. Reducing the potential to 0.66V resulted in crystals of BKBO that were nonsuperconducting, and reddish/bronze in color. Below is the graph Han *et al.* reported for composition *vs.* overpotential (Figure 3).

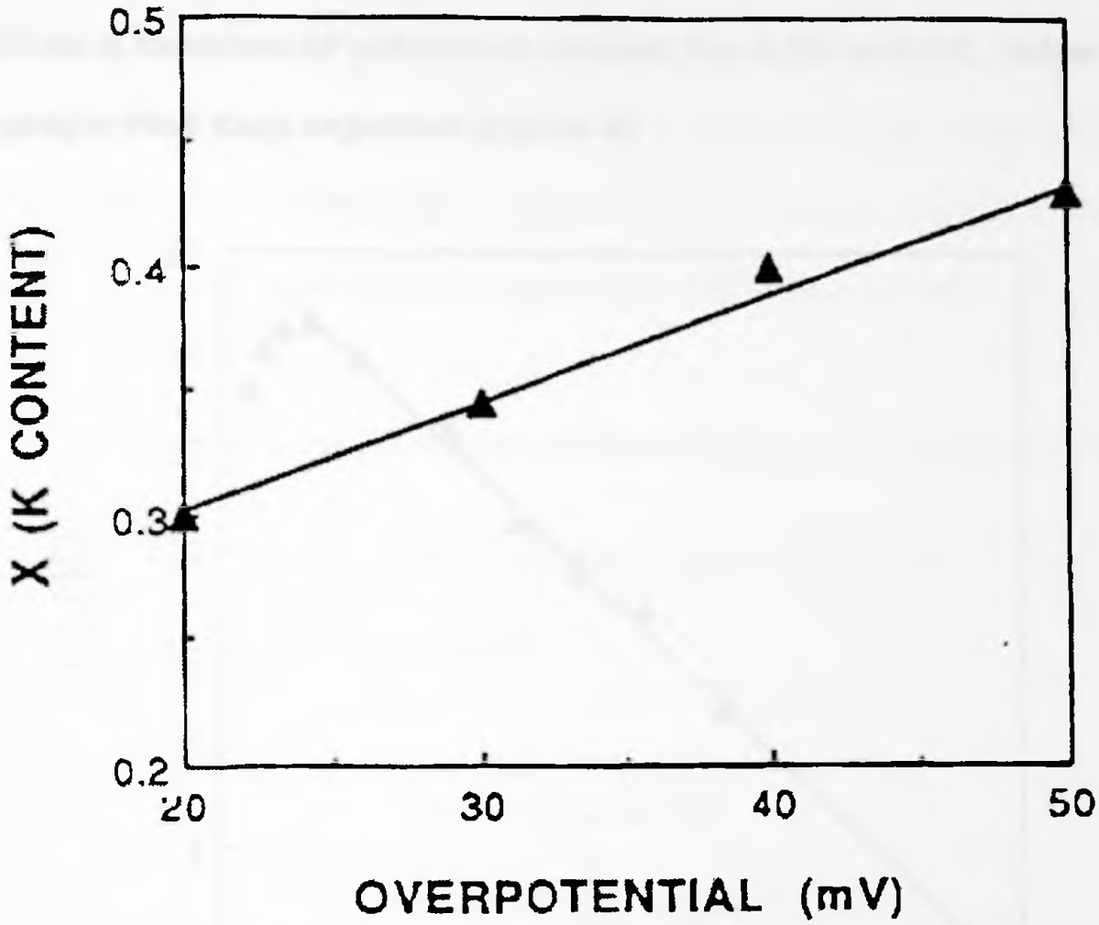

Fig. 3, Potassium content *vs.* overpotential for BKBO.

They also reported the T_c for the different compositions of BKBO as a function of potassium content for 0.35<x<0.55. Below is the graph that they reported (Figure 4).

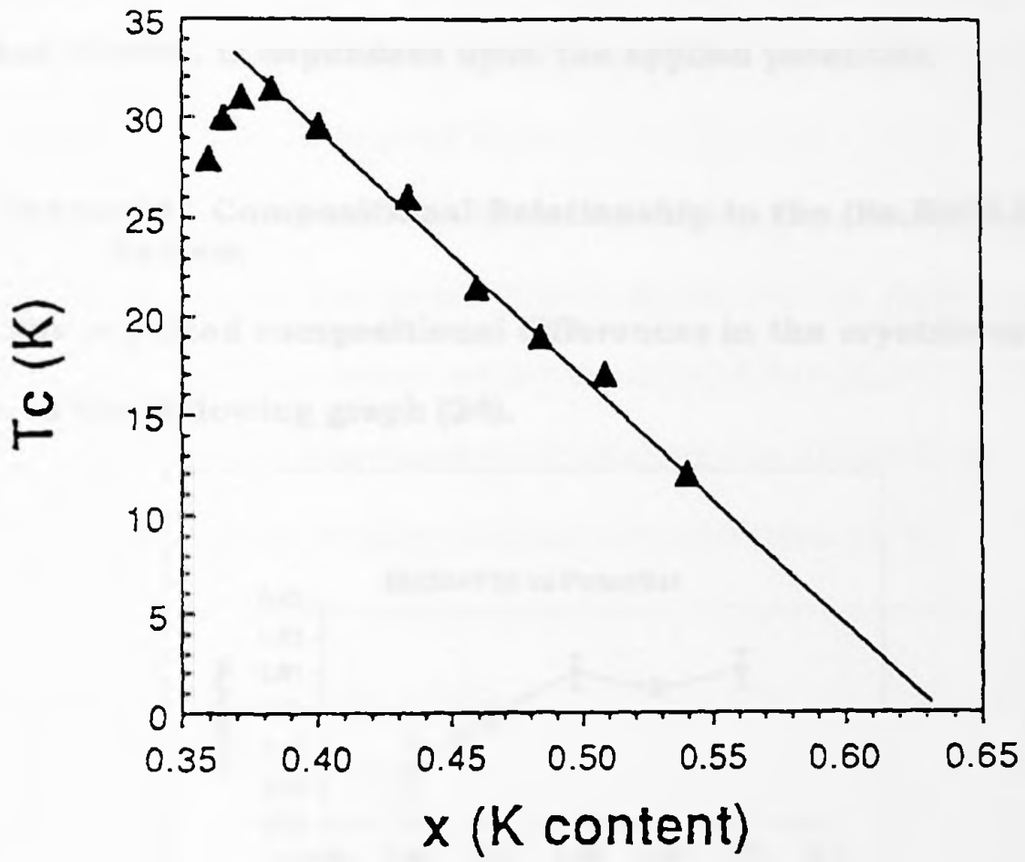

Fig. 4, T_c *vs.* potassium content for BKBO.

Electrodeposition of $Ba_{1-y}K_yBi_{1-x}Pb_xO_3$ (BKPBO)

A related compound has also been investigated by the Norton group. Bin Zhuang studied the effect of different applied potentials on the growth of BKPBO (23). Again the composition, and thus the T_c of the crystal, is dependent upon the applied potential.

Potential - Compositional Relationship in the $(Ba,K)(Bi,Pb)O_3$ System

The reported compositional differences in the crystals are shown in the following graph (24).

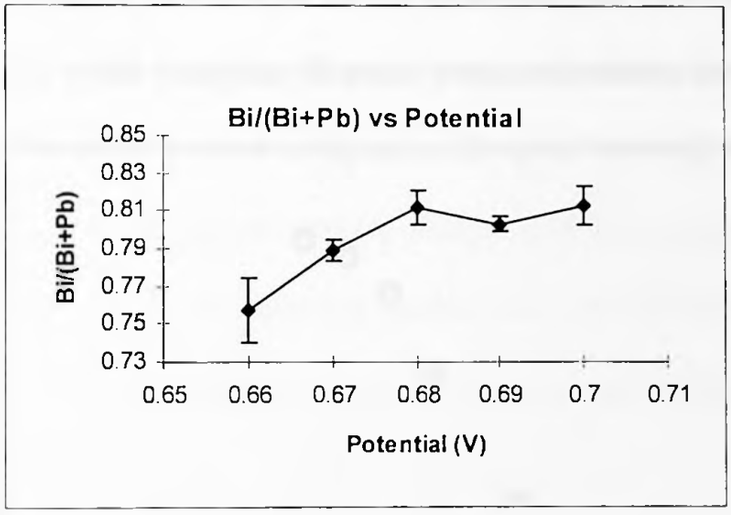

Fig. 5, Composition of BKPBO *vs.* potential

According to the graph, the difference was greatest between 0.66V and 0.68V potentials. Because of the difference in the composition, these potentials were decided to be the endpoints of the cycle for multilayered growth. Potentials higher than 0.68 V

would produce little compositional difference, and increase the possibility of unwanted structural defects in the final crystal. Potentials lower than 0.66V would increase the amount of time necessary to grow the layer at lower potential, or worse, might produce no growth at all. T_c ranged from 11.2 K for growth at 0.68 V, to 13.8 K for growth at 0.66 V.

Marx *et al.* measured the T_c *vs.* the total potassium plus lead concentration (25). In the graph (Figure 6), the circles represent literature values of the onset resistivity data of $Ba_{1-x}K_xBiO_3$. The squares and triangles represent their observation of the T_c of $Ba_{1-y}K_yBi_{1-x}Pb_xO_3$ with varying dopant concentration (x+y).

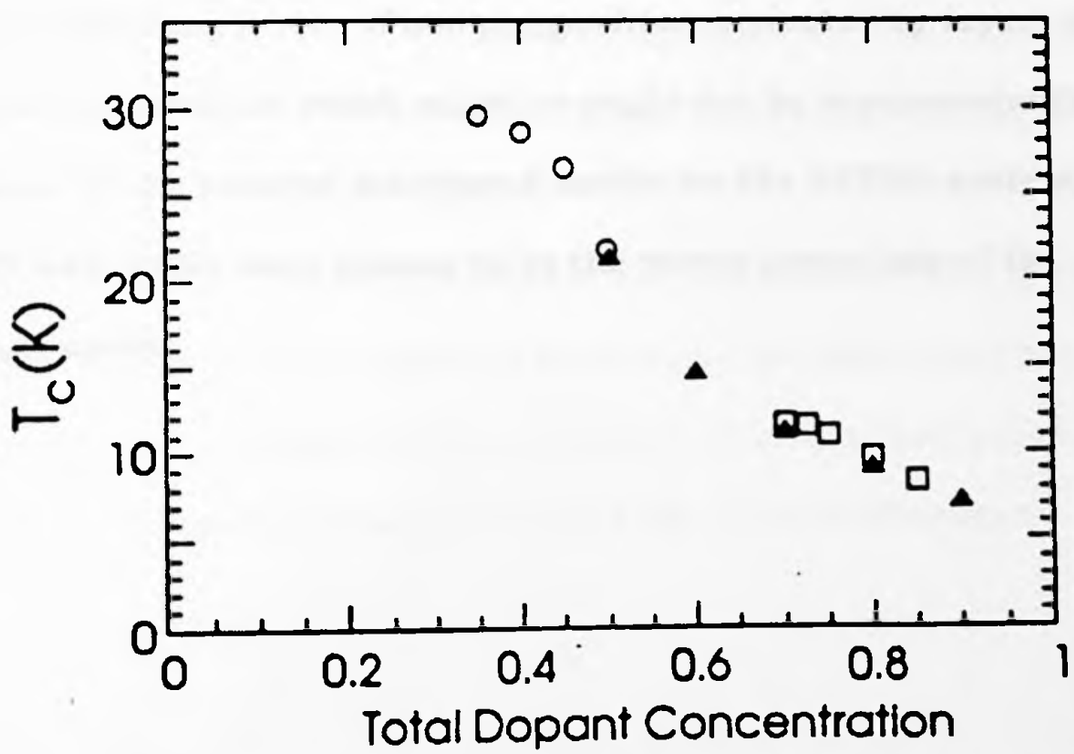

Fig. 6, T_c *vs.* total dopant concentration in $Ba_{1-y}K_yBi_{1-x}Pb_xO_3$.

Project Objective

Both of the electrodeposition studies of BKBO and BKPBO suggest that it may be possible to create a layered crystal with spatially modulated compositions by changing the potential during growth. Each compositional layer would have a different T_c, or perhaps one would be a superconductor, and the second not superconducting at all.

This, then, was the basis of this research. The object was to create a crystal that was modulated compositionally by changing or cycling the applied potential during the deposition of the crystal. This compositionally modulated crystal would contain superconducting layers of one composition separated by layers of a second composition which might or might not be superconducting. Because of the reasons mentioned earlier for the BKPBO system, 0.68V and 0.66V were chosen to be the vertex potentials of the voltage cycle.

Materials and Methods

Electrochemical Equipment

Potentials were maintained with a model 363 EG&G Princeton Applied Research potentiostat. The programmed potential was produced by a Keithley 220 programmable current source connected to a 10 KΩ resistor. The potentiostat tracked the potential drop across the resistor, which was connected to its external input. The potential was monitored using a Hewlett-Packard 3478A multimeter, and current output was recorded with a Linear Instruments Corp. model number 355 chart recorder. Heating was provided by a heating mantle connected to a 120 volt Staco Energy Products Co. type 3PN101 variable autotransformer. Constant temperature was maintained using a model CN-310 Omega temperature controller. (Figures 7 and 9: Pages 14 and 19)

Two types of Teflon crucibles (Cole Parmer) were used in the experiments. Initial experiments were performed with crucibles measuring 3.5 cm high x 2.5 cm diameter. In later experiments, the crucible size was increased to 7.0 cm high x 8.0 cm diameter.

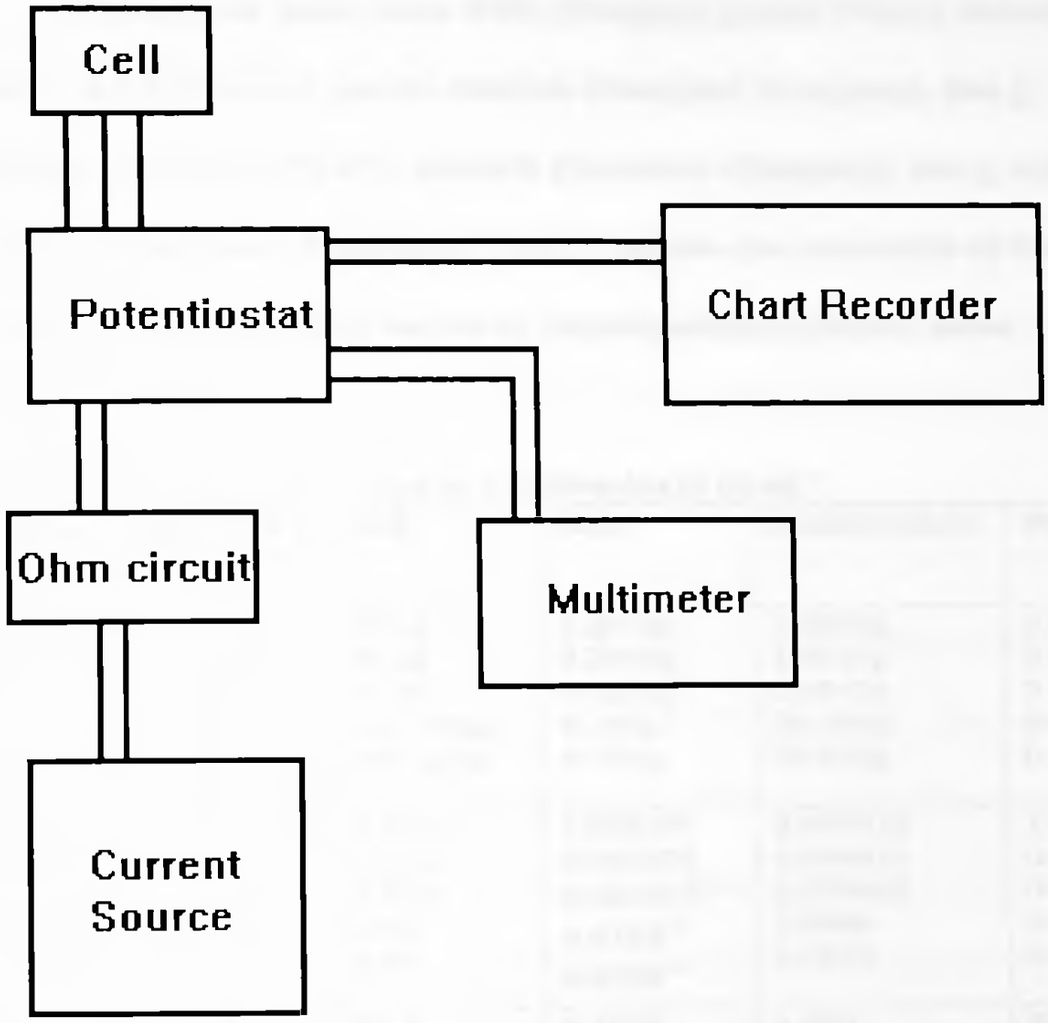

Fig. 7, Block diagram of the electronic equipment used.

Chemicals Used and Molar Ratios in Solution

Chemicals used were KOH (Reagent grade; Fisher Scientific), Bi_2O_3 (ACS reagent grade; Aldrich Chemical Company, Inc.), $Ba(OH)2•8(H_2O)$ (99.9%; Aldrich Chemical Company, Inc.), and PbO ('Baker Analyzed' Reagent). Table 1 shows the amounts of the chemicals used in the series of experiments reported here.

Table 1; Chemicals Used.*

Starting material	Experiment number	KOH	Bi_2O_3	$Ba(OH)_2·8(H_2O)$	PbO
Grams Used	1) 2) 3) 4) 5)	20.0g 20.0g 20.0g 350.091g 350.227g	0.2012g 0.2495g 0.4568g 8.775g 9.786g	1.4544g 1.4547g 1.4541g 25.480g 25.539g	0.0390g 0.0 0.0 0.0 0.0
Moles of metals in solution	1) 2) 3) 4) 5)	0.310 0.310 0.310 5.42 5.42	8.64E-04 0.001071 0.001073** 0.0188** 0.0188**	0.004610 0.004611 0.004609 0.0808 0.0810	1.75E-04 0.0 0.0 0.0 0.0
Molar ratio of metals in solution	1) 2) 3) 4) 5)	67.2 67.2 67.2 67.1 67.0	0.1874 0.2322 0.2327** 0.2325** 0.2321**	1.000 1.000 1.000 1.000 1.000	0.0380 0.0 0.0 0.0 0.0

* **Cycle times for the experiments are listed in Table 2.**

** **Bi_2O_3 has a solubility limit of 0.25g per 20.0g of KOH at 260 °C. This ratio was used in calculating the number of moles in solution and the molar ratio. (26)**

Electrodeposition Procedure

KOH, which contains 10% to 15% water by weight as delivered from the manufacturer, was placed in the Teflon crucible. Then the power was applied to the heating mantle. The KOH was allowed to heat to melting (approximately 180 °C), then the $Ba(OH)_2 \bullet 8H_2O$ was added to the molten KOH with stirring. This was done to reduce the splattering that followed from the evaporation of the hydrated water in the $Ba(OH)_2 \cdot 8H_2O$.

When a temperature of 260 °C was obtained, the Bi_2O_3 was added. The solution was stirred for 15 min., after which, the melt was then covered, and water saturated inert gas (nitrogen) flow was initiated. The delay in the addition of the Bi_2O_3 was to minimize the amount of time that the complete Bi^{3+} containing flux was exposed to air. Nitrogen provides an inert atmosphere to prevent oxidation products from forming through reaction with atmospheric oxygen.

Because the KOH contained 10% to 15% water by weight, the melting point of the solid was depressed from 360 °C to approximately 180 °C. If the nitrogen had been dry, there would have been the possibility for the surface of the melt to become sufficiently deficient in water to form a solid cap. This cap would hinder crystal growth and the harvesting of any crystals that formed.

After covering the crucible and attaching the nitrogen line, the melt was allowed to further stabilize for at least one hour. During this time the electrodes were cleaned using concentrated nitric acid and then rinsed with distilled water. Approximately 30 mL of concentrated nitric acid was placed in a 50 mL beaker to be used to wash the electrodes. Each of the silver electrodes was immersed in the nitric acid for 30 to 60 seconds, and rinsed with distilled water. This was repeated until there was no visible contamination on the electrodes. Then the bismuth electrode was cleaned in the same manner using less than 5 seconds of immersion in nitric acid, then rinsing with distilled water. This order was repeated in each experiment. This was to prevent any possibility of contamination of the silver electrodes. Contamination of the bismuth electrode was not as large a concern because any silver nitrate on the bismuth electrode would be removed when the electrode was rinsed with distilled water.

One of the silver electrodes (the working electrode) was positioned in a Teflon holder. For use with the small crucible, the holder was a small, flexible Teflon tube that slid over the electrode. For the large cell, the holder was a 10 cm long by 1.5 cm diameter Teflon rod that had a hole drilled through it lengthwise (Figure 8).

Fig. 8, Teflon holder for large cell.

The electrode was positioned in two different ways. In the first experiment it was extended by 0.5 cm from the bottom of the Teflon tube. In later experiments, the electrode was positioned flush to the Teflon holder. The change was made in an attempt to minimize the nucleation sites, thus providing larger (although fewer) crystals. Producing a smaller number of crystals would also reduce the amount of solvated ions that were removed from solution, thus helping to preserve solution stoichiometry throughout the experiment.

The electrodes were placed in solution sequentially. First, the negative electrode was placed in solution, extending 1 to 3 cm. below the surface of the solution. Second, the Bi (reference) electrode was placed in solution, again extending beneath the solution 1 to 3 cm. Finally, the working electrode in the Teflon holder was placed in the solution. It was situated so that the tip of the exposed electrode (protruding out of the holder or flush) was 2-3 cm. below the surface of the melt. (See Fig. 9 for details of cell setup.)

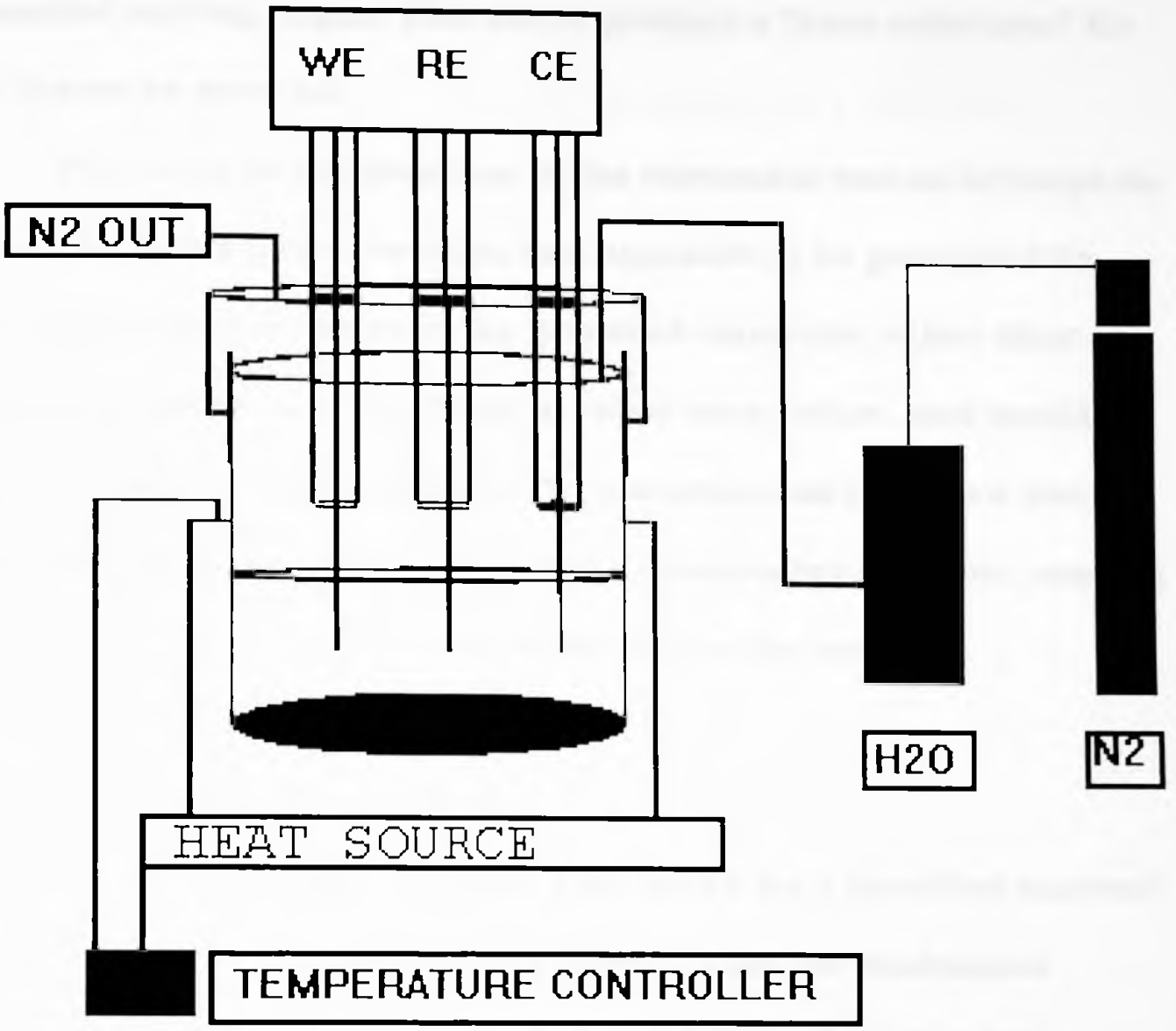

Fig. 9, Details of cell. WE = Working electrode, RE = Reference electrode, CE = Counter electrode (negative electrode).

Immediately after the insertion of the electrodes, the potentiostat was connected to the electrodes and current (at 0.68V) was allowed to flow. This usually resulted in the immediate darkening of the working electrode as microcrystals started to form. Crystals were grown for a specified amount of time at 0.68V before

potential cycling began. This was to produce a "base substrate" for the layers to grow on.

The order of the insertion of the electrodes was an attempt to avoid the formation of crystals that appeared to be generated by solubility characteristics of the dissolved materials rather than electrochemical reaction. These crystals were yellow, and would grow on each of the electrodes. The electrodes may act as a heat sink, reducing the temperature of the surrounding solution, causing the insulating material to crystallize on the electrodes.

Depositing Modulated Materials

Initially the BKBO crystals were grown for a specified amount of time at 0.68V. This provided a substrate for the modulated growth. The potential was switched to 0.66V, and cycling was continued throughout the remainder of the growth period.

Harvesting the Crystals

Harvesting the crystals was a simple matter of removing them from the melt, allowing them to air cool for approximately 30 minutes, and finally rinsing with distilled water. If the silver working electrode had been allowed to extend beyond the Teflon holder, the crystals were left on the electrode during the initial washing, and then later removed. A final wash was performed by

placing the crystals in a small beaker and adding 30 to 50 mL of distilled water. The beaker was gently swirled for 5 min. The crystals were then removed and set aside to dry. Ultrasonic cleaning was not used to clean the crystals.

If the electrode was flush with the Teflon holder, the crystals were removed prior to washing. In this configuration the crystals did not adhere to the electrode as well, and could fall off at an inopportune moment. For crystals grown flush with the holder, all washing was done in a beaker with multiple rinsings of distilled water, then set aside to dry.

Crystal Polishing Procedure

The crystals are cubic and grow with equal speed in three dimensions. This has the effect of producing single crystals with modulation from the center outward (See Figure 10).

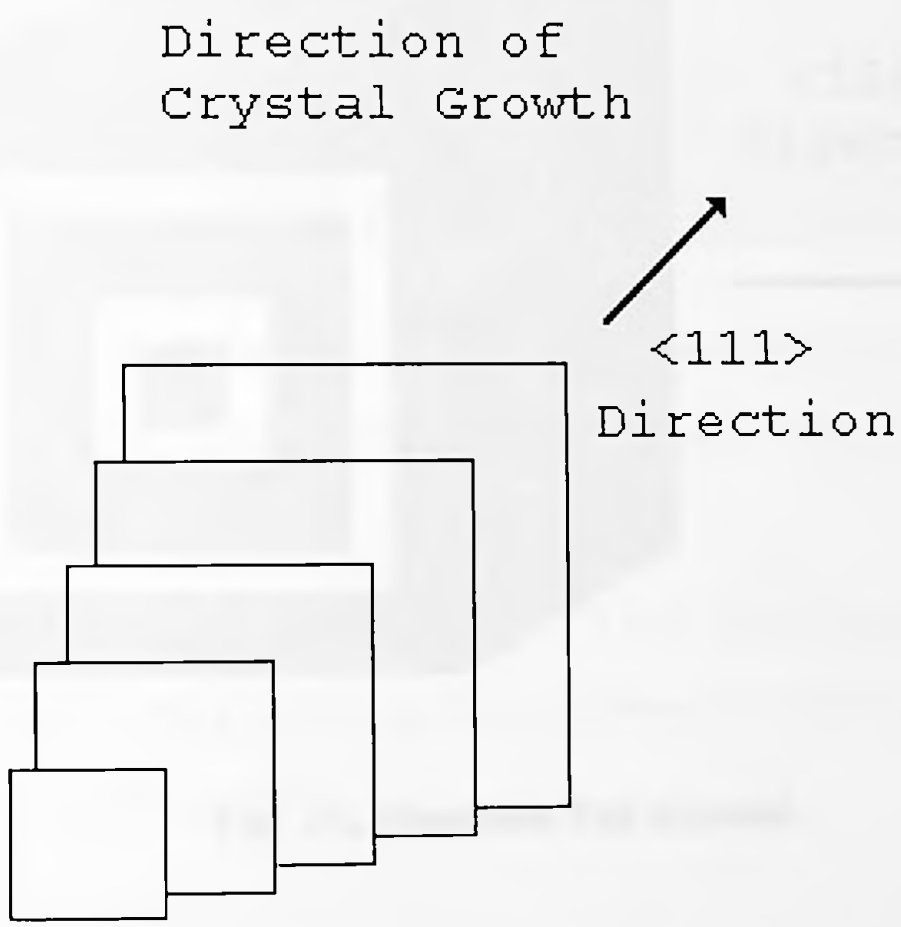

Fig. 10, Showing the direction of crystal growth.

Thus when the crystal grows, each layer completely covers its predecessor, creating alternating "cubic shells" that surround the previous growths. Thus, when viewing an uncut crystal modulated in this fashion, it appears to have only one composition, the composition of the surface (Figure 11).

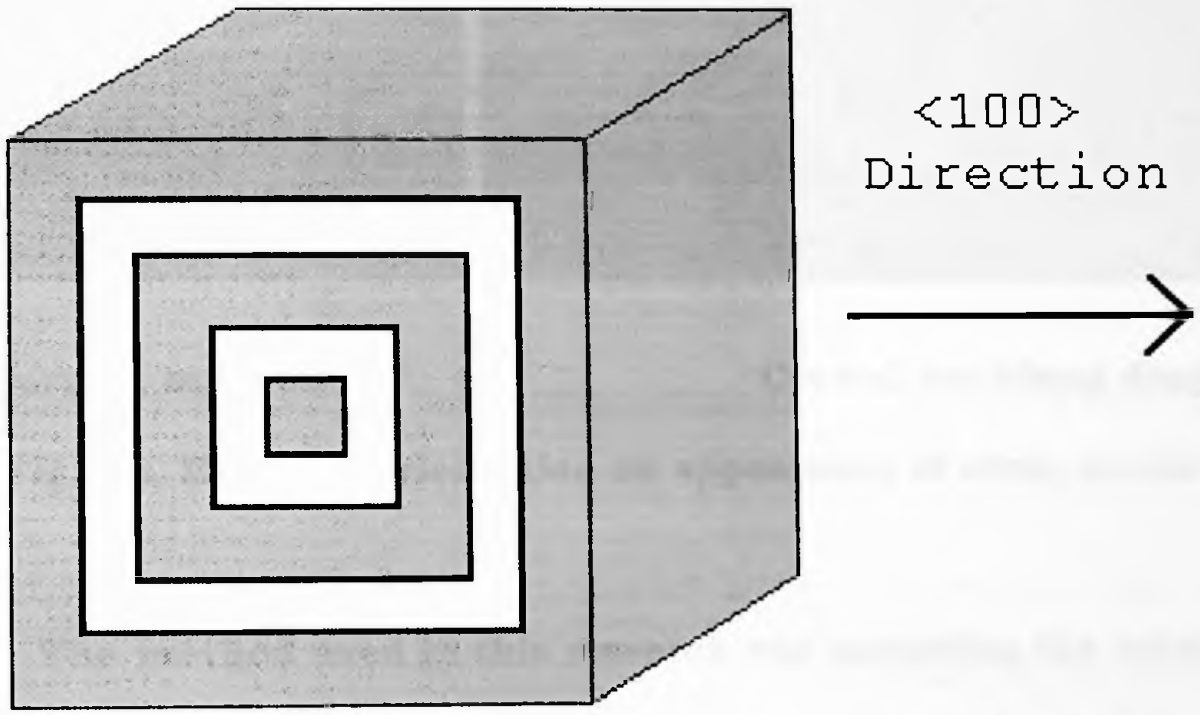

Fig. 11, Idealized Cut Crystal.

In order to view the modulation of the crystal, it is necessary to somehow cut into the crystal. The cut must be as close to parallel to a face of the crystal as possible. If it is not, then the width of the modulation will be abnormally elongated along two sides (Figure 12).

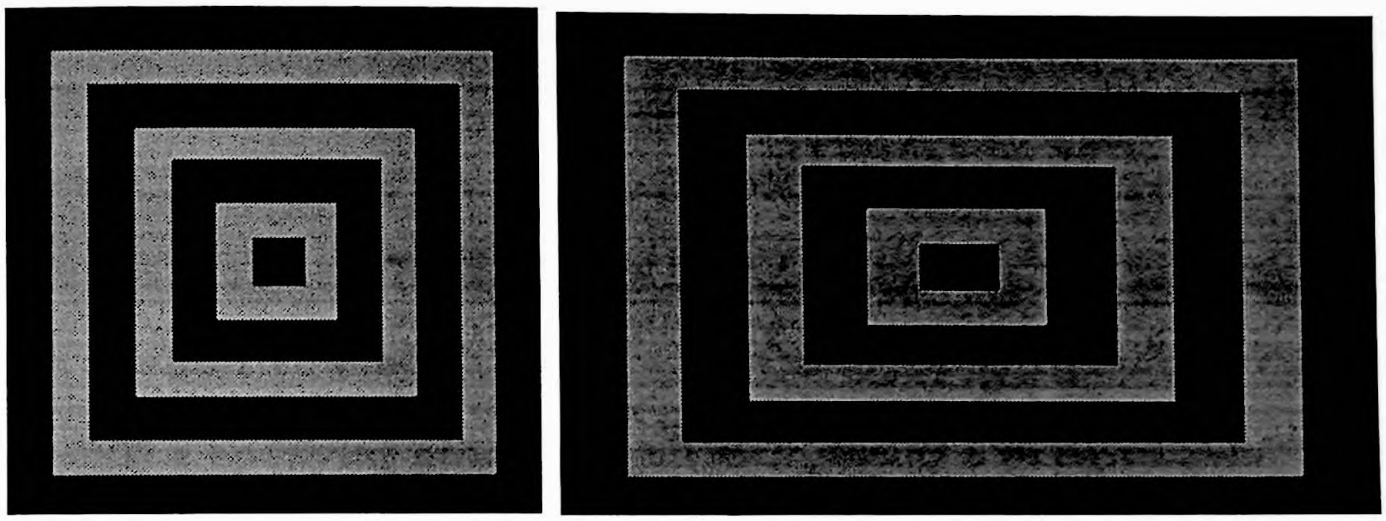

Correct orientation Crystal cut along diagonal

Fig. 12, Effect of orientation on appearance of cross section.

The method used in this research was mounting the crystal in a Bakelite ring using epoxy, grinding it down to the desired depth, then polishing it smooth.

Mounting the Crystal in the Bakelite Rings

The crystals grew in clumps on the electrode. Even with the naked eye, single crystals were apparent on the electrode. A binocular, low power microscope was used to identify crystals with well developed faces. Usually crystal selection was performed immediately after the harvest. The binocular microscope was also used in the cutting and polishing procedure to intermittently monitor progress. Thus, the low power microscope was used mainly as a qualitative tool.

The epoxying process began with placing a water-soluble separator gel on a 3 x 1.5 inch glass slide. An even covering was obtained by taping the long edges of the slide down with cellophane tape. The gel was then placed across one of the smaller sides and it was spread across the rest of the glass slide by using the edge of a second slide. This usually produced an even coating of the gel on the initial slide (Figure 13).

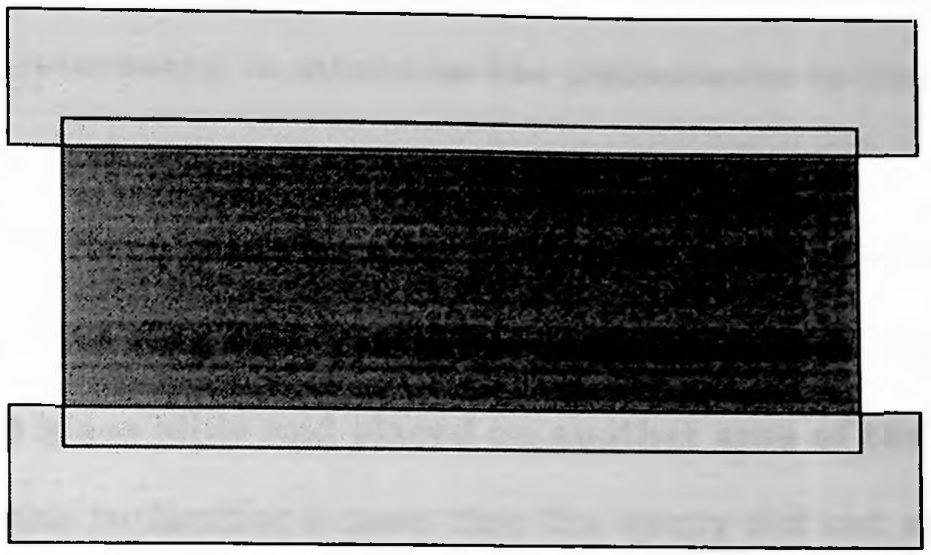

Fig. 13, Slide Taped to Counter Top.

The crystals were inspected under the low power optical microscope to determine the best side to be exposed to the polishing procedure. The side chosen was usually the side that was most flat. The crystal was then placed in the center of the gel coated slide with the chosen side down, in the gel. A $1^1/_4$ inch diameter by $^3/_4$ inch tall Bakelite ring was positioned on the slide so that the crystal was at the center of the ring.

Workman Double Barrel "5 Minute" Epoxy was used to mount the crystals. Enough epoxy was used to cover the crystal and evenly fill the lower portion of the Bakelite ring about $^1/_4$ of an inch deep. It was mixed so that as few air bubbles as possible were formed. After mixing, the epoxy was transferred to the Bakelite ring using the large end of a pasture pipette. The pipette was used to transfer

the epoxy because the epoxy flowed very slowly and smoothly from it. This was necessary to minimize the disturbance to the crystal in the separator gel.

Ten to fifteen minutes after mixing the epoxy, the entire epoxied Bakelite ring and crystal were separated from the original place on the glass slide and placed on another area of the gel coated slide. This was to further ensure that the epoxy did not stick to the glass slide. The epoxy was allowed to sit overnight to ensure that all areas were fully cured. The next day, the mounted (epoxied) crystal was removed from the glass slide. It was then rinsed with distilled water to remove the separator gel.

If a crystal was to undergo STM characterization, a slight modification to the above procedure was necessary. The STM depends on a conductive sample. Mounting the crystal to the STM is made easier if a larger contact pad can be created. This was readily achieved by covering the crystal with a conductive epoxy (2400 Circuit Works Conductive Epoxy Kit) before using the five minute epoxy. The epoxy would flow over the crystal and create a conductive surface around the crystal. The conductive epoxy was allowed to cure, then the procedure would continue as described above.

Grinding and Polishing the Epoxied Crystals

The best method for viewing the interior of the crystal was found to be a grinding and polishing procedure. The grinding process removed approximately 1/4 to 1/2 of the crystal. This surface was then polished with consecutively smaller aluminum oxide polishing solutions.

The initial grinding was done with 400 grit silicon carbide sandpaper. Caution is advised during this procedure. Too much pressure will fracture the crystal, possibly dislodging the crystal from the epoxy. Also, if the crystal is ground too thin, it will begin to fracture. After the initial grinding, 600 grit sandpaper is used to help smooth out the surface.

Polishing began with the use of 5 micron aluminum oxide polish. Again, care must be taken not to use too much pressure, although polishing the specimen too thin is not as large a concern. After approximately fifteen minutes of polishing with the 5 micron polish, many individual layers could be observed under the optical microscope. Polishing continued using 1 micron, 0.5 micron, 0.1 micron, and finally 0.03 micron grit polishes. The polishing was performed by hand, usually for five to fifteen minutes for each grade of polish.

Microscopy and Images

The variation in the color of the component layers in the crystals was used to measure the modulation. Without magnification, the polished crystals appeared deep blue with tinges of orange and red in them. The multilayered BKBO crystals were viewed by using a low power microscope, a reflectance microscope (ausJENA), a scanning tunneling microscope (Nanoscope II), and SEM (scanning electron microscope).

The reflectance microscope was used mainly after the polishing was accomplished. This was the major method of sample observation and imaging. The reflectance microscope was able to easily distinguish between the layers, and provided sharp images.

To obtain optical images in digital format, the reflectance microscope was fitted with a Sony DXC-107 CCD camera. The image from the CCD camera was captured by a 386 computer equipped with a WinVisionPro image capturing board. The board was controlled by Photofinish, a commercial image capturing and editing program.

Results and Discussion

Optical imaging

Modulated (Ba,K)(Bi,Pb)O_3

Based on the work of Bin Zhuang, an earlier group member, crystals of (Ba,K)(Bi,Pb)O_3 were grown using dual potential. Times for the vertex potentials were chosen based on approximate calculations from crystals grown earlier in this research without modulation. These nonmodulated crystals were grown from 20 mL of a solution with the same composition as experiment #1 (see table 1).

The first single potential experiment used in these calculations produced 0.0035g of (Ba,K)(Bi,Pb)O_3 after 1.5 hours at a potential of 0.66V with the electrode protruding 0.6 cm below the Teflon holder. This produced a growth rate of approximately ((0.0035g) / (1.5 hr * 3600s per hr * 0.6 cm)) = 1.08E-6 g/cm*s.

The second single potential experiment used in these calculations produced 0.0283g of (Ba,K)(Bi,Pb)O_3 after 3 hours at a potential of 0.68V with the electrode protruding 0.55 cm below the Teflon holder. This produced a growth rate of approximately ((0.0283g) / (3 hr * 3600s per hr * 0.55 cm)) = 4.76E-6 g/cm*s.

The approximate density of BKPBO was based on a calculation of $BaBiO_3$, using a roughly estimated 4.25 Å unit cell parameter. The molar weights of Ba (137 g/mol), Bi (209 g/mol) and O_3 (48 g/mol)

were added together and divided by Avogadro's number. This gave an approximate weight of the unit cell (6.6E-22g). Dividing this by the estimated volume of the unit cell (4.25E-8 cm)^3 gave a rough estimate of the density of $BaBiO_3$ (8.6 g/cm^3).

The silver wire used for deposition had a radius of approximately 0.05 cm. In order to be observable under the optical microscope, a growth thickness on the order of 0.001 cm (10 microns) was desired. This would make the total radius of the silver wire and the crystal growth 0.051 cm. The volume of the growth would be $V_{crystal} = \pi r_2^2 h - \pi r_1^2 h$ (Where r_1 = radius of the silver electrode (0.05 cm), r_2 = the radius of the silver electrode and the deposited crystal (0.051 cm), and h = the length of the electrode in solution (assumed to be 1 cm in this estimation)). The volume of the deposited crystal (for 0.001 cm radius) would be 3.17E-4 cm^3.

Multiplying the volume of the deposited crystal (3.17E-4 cm^3) by the calculated density for $BaBiO_3$ (8.6 g/cm^3) produces an estimate of the mass in grams that would be theoretically deposited (2.73E-3g). The theoretical weight was then divided by the growth rates calculated above for each individual potential (1.08E-6 g/cm*s for 0.66V and 4.76E-6 g/cm*s for 0.68V) again using 1 cm for the theoretical length of the electrode in solution. This should give approximate times for deposition at each potential to create layers

on the order of 0.001 cm. The times from the above calculation are 2528 seconds at 0.66V and 574 seconds at 0.68V.

The actual times used were 2160 seconds (36 minutes) for 0.66V and 576 seconds (9.6 minutes) for 0.68V. The reasons for the differences were because of ease of programming the constant current source, and translation of times into minutes.

The (Ba,K)(Bi,Pb)O_3 crystals were grown using the above times, mounted in epoxy, then ground and polished as earlier described. The reflectance microscope was used to image the polished crystal. The microscope images displayed a barely discernible repeating pattern in cross section. Image filtering techniques were unable to enhance the contrast between the layers (Figure 14).

If it is assumed that the smaller layer is the 0.66 V growth (it was grown at a significantly shorter time than calculated), and the larger layer is 0.68 V. Then a ratio of the actual times to the calculated times should equal the ratio of the distances.

For 0.66 V:
$2160s/2528s = X\mu/10\mu : X = 8.54\mu$

For 0.68 V:
$570s/574s = X\mu/10\mu : X = 9.93\mu$

(X = the theoretical distance for the experimental times.)

Although the actual distances are different (see Table 2, page 46), they ratio very well to the theoretical calculation.

$8.54\mu/9.93\mu * 6.89\mu = 5.93\mu \approx 6.06\mu$

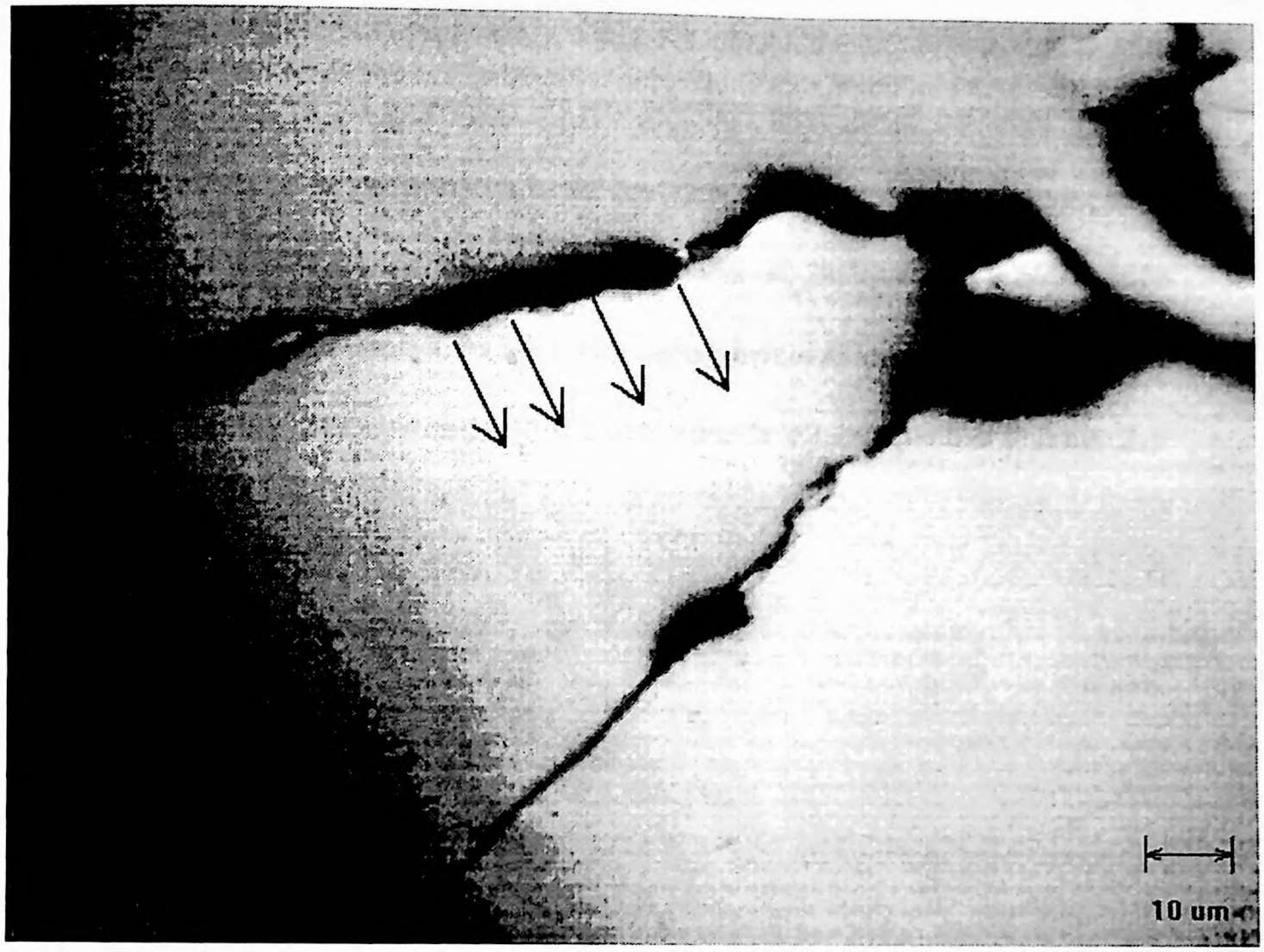

Fig. 14, Optical image of multilayered BKPBO.

Because optical differentiation was the primary method of choice for distinguishing between layers of different composition, and the two phases of $(Ba,K)(Bi,Pb)O_3$ would become superconducting at reasonably close temperatures (13.8 K for 0.66V growth and 11.2 K for 0.70V growth) (27), a related, but better suited chemical system was adopted for creating modulated lattices.

The new approach would not incorporate lead in the growth of the crystals. This method was based on prior work of our group, and the recently reported results of Han *et al.* (28)

Modulated $(Ba,K)BiO_3$

The layers in crystals of $(Ba,K)BiO_3$ had good optical definition. The layers were blue for the superconducting phase, and reddish for the nonsuperconducting phase. Below is a gray scale representation of one of the first color optical images obtained of the layered BKBO system. (This is growth #2 in Tables 1 and 2.)

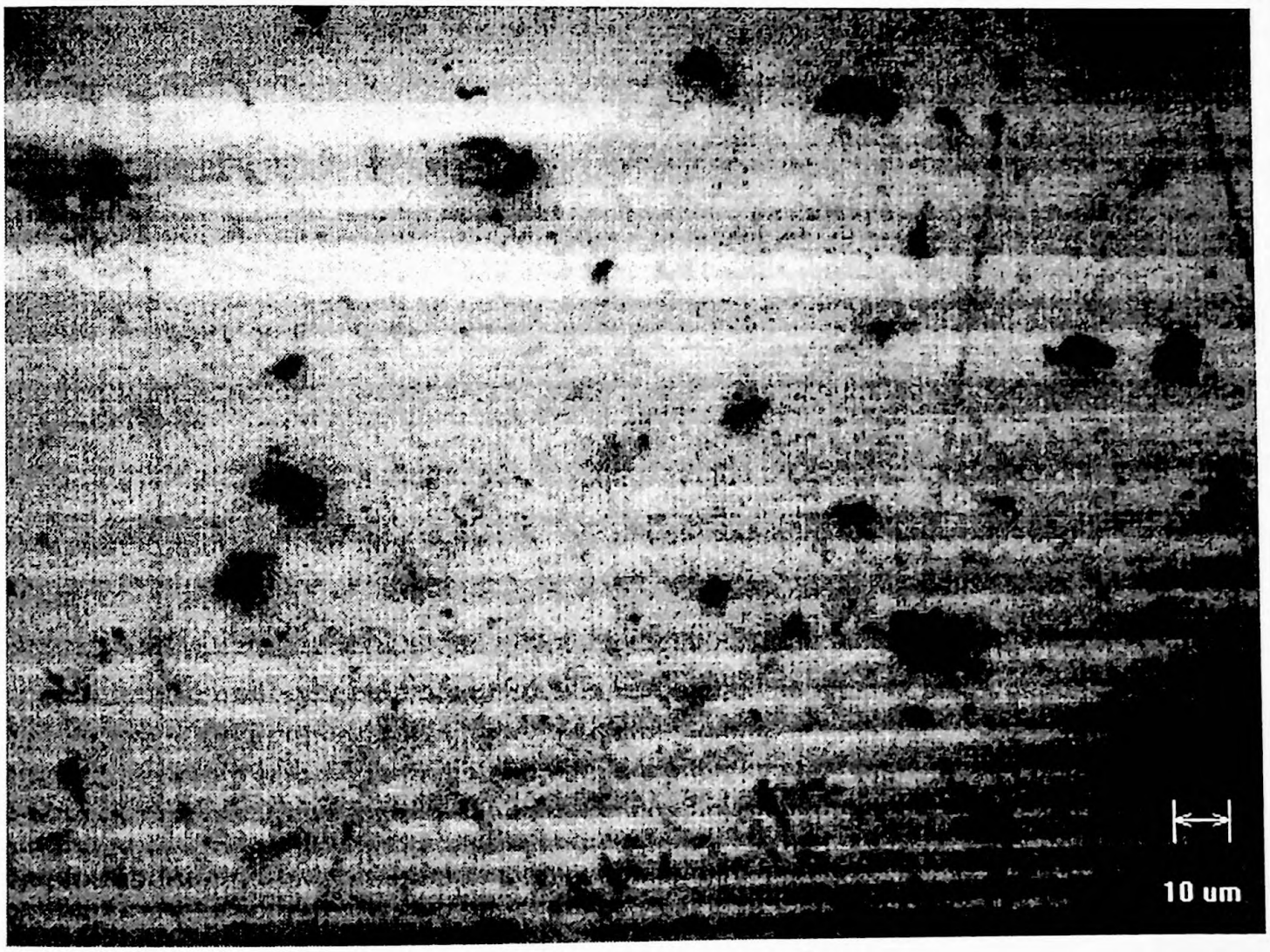

Fig. 15, Image of multilayered BKBO.

In Figure 15 the red nonsuperconducting layer appears as the lighter shade. The blue superconducting layer appears as the darker shade.

In the first experiment with BKBO, the cycle times were chosen based on the previous experiments with the BKPBO system (2160 seconds for 0.66V and 576 seconds for 0.68V). The times were such that the layers were approximately the same thickness. The potential - phase relationship for the layers was made definitive in the second modulated BKBO experiment.

In experiment 3, the deposition times were equal (2160 seconds for both potentials). Because the phase grown at higher potential is faster, (increased current) the phase grown at 0.68V should be the largest. This is shown in the following image.

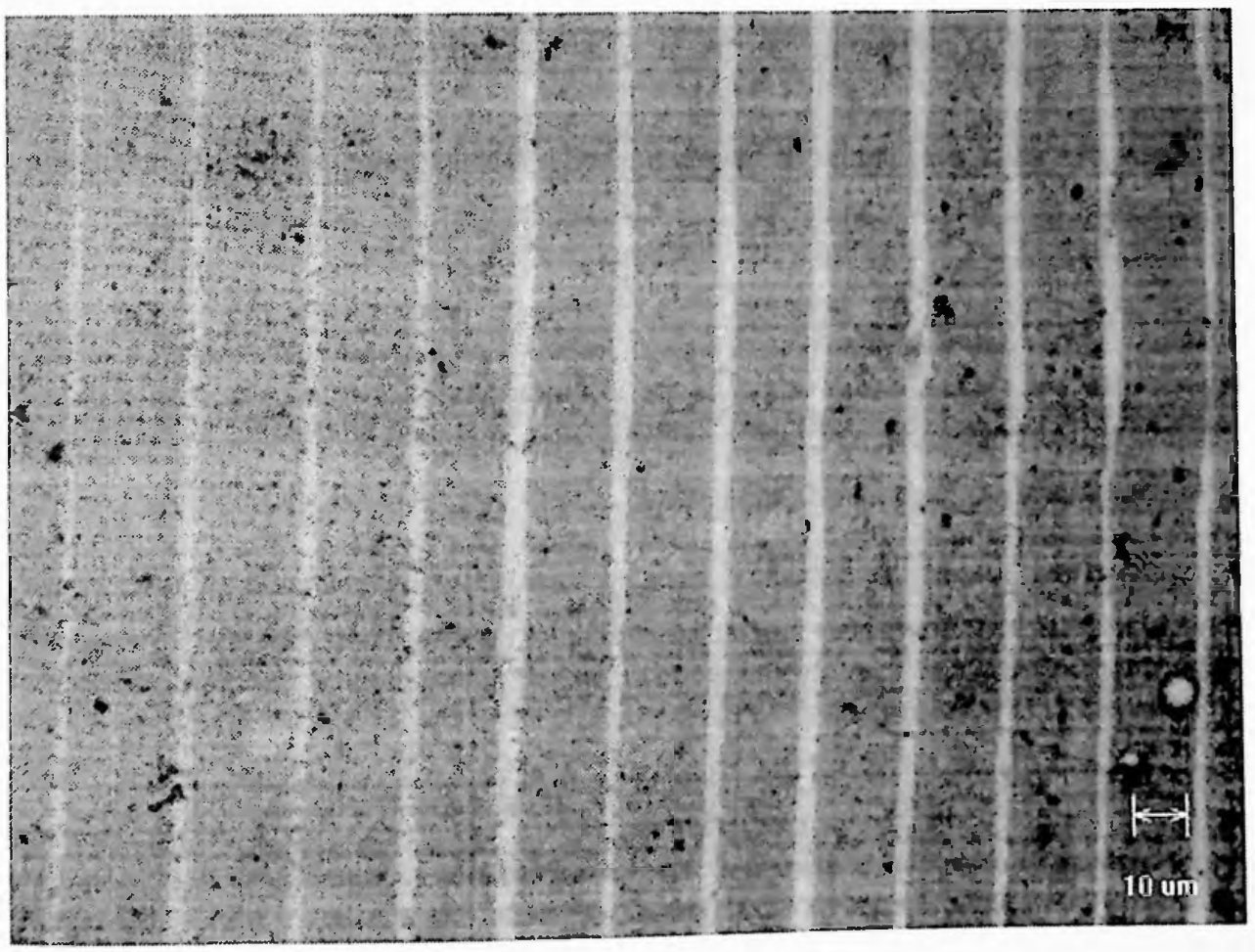

Fig. 16, Gray Scale of BKBO grown with equal time for each cycle. (Color version is on the dedication page.)

(Picture quality has increased mainly because of increased experience with the image capturing equipment.)

Again, the red nonsuperconducting layer appears as the lighter shade. The blue superconducting layer appears as the darker shade.

In order to more carefully characterize the optical properties of the layers, an image of growth number 4 (see Tables 1 and 2, pages 14 and 46) was converted to gray scale, and pixel intensity was plotted. Figure 17 was the image analyzed. The data obtained, an average of 25 pixels (approximately 7.5 microns) on either side of the lines, is plotted in Figures 18 and 19.

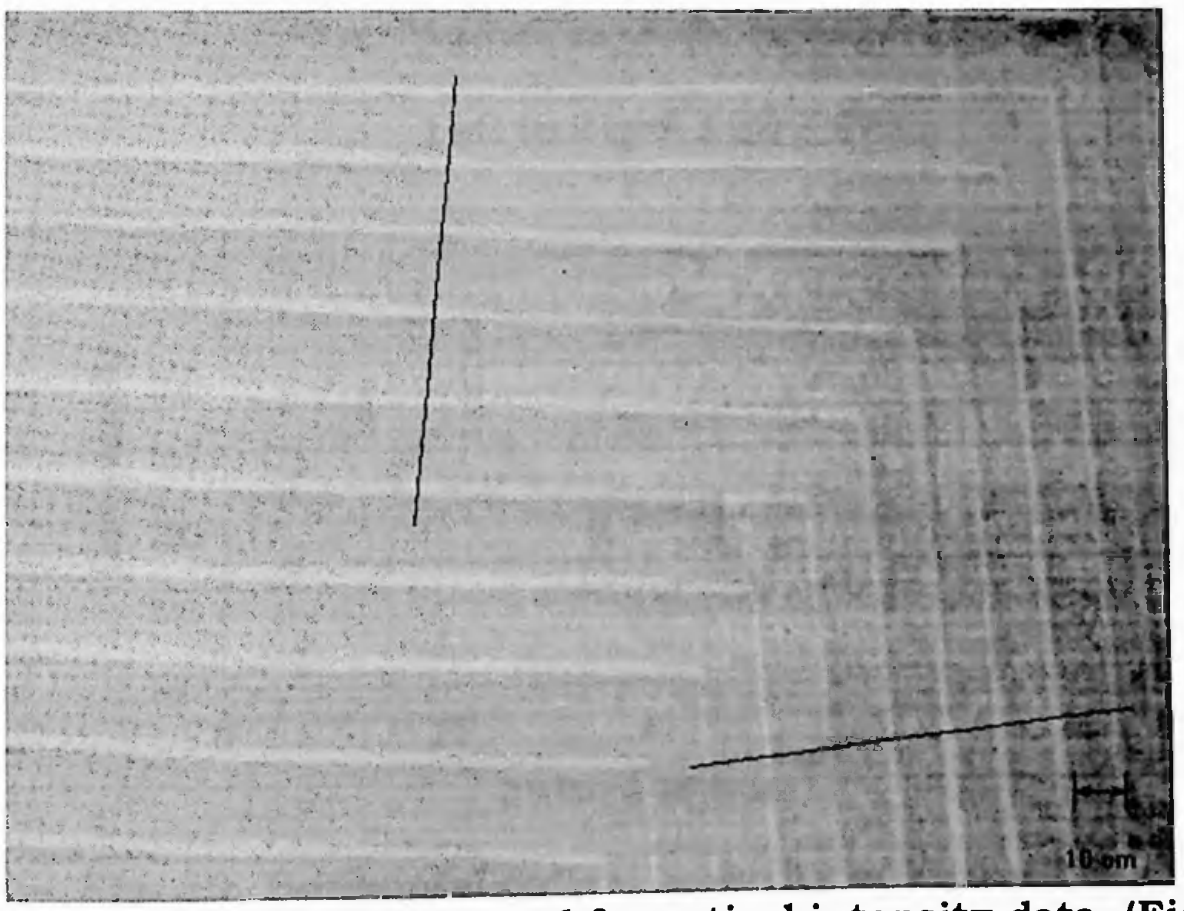

Fig. 17, Gray scale of image used for optical intensity data. (Figures 18 and 19.) Lines indicate where data was obtained.

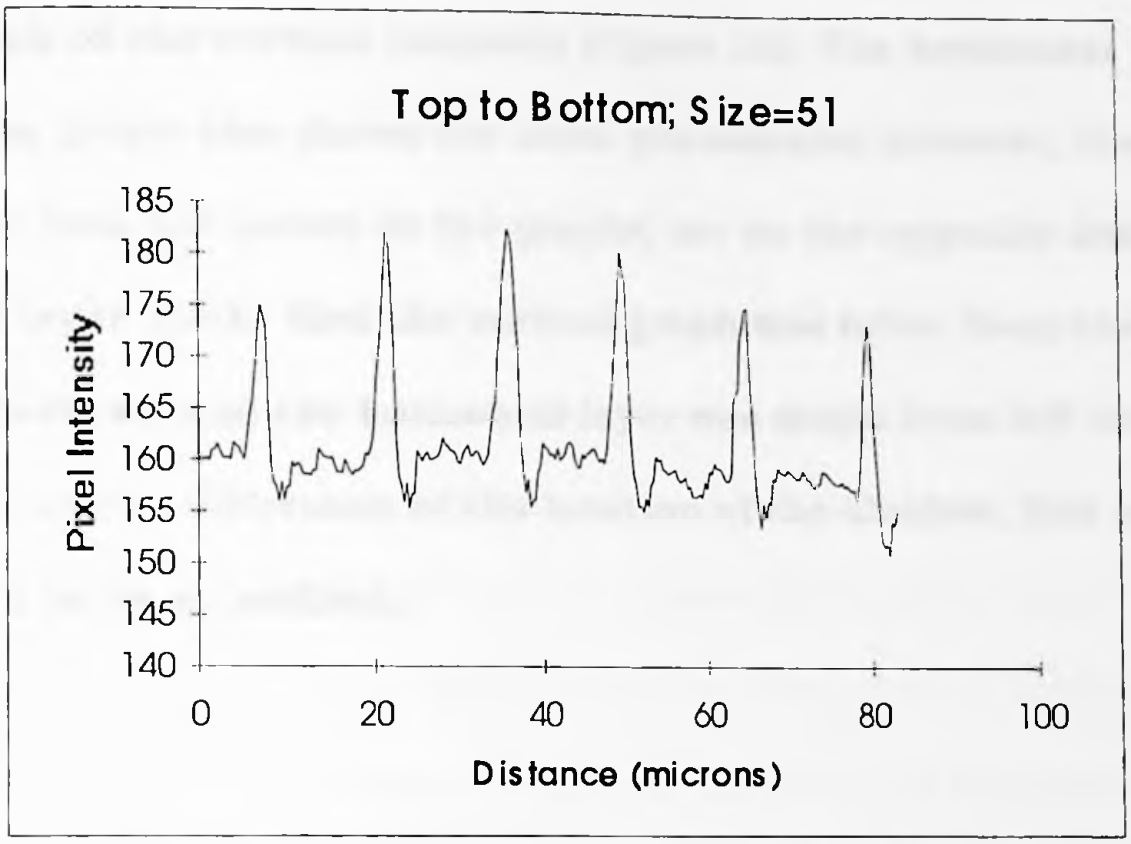

Fig. 18, Vertical optical intensity of Figure 17.

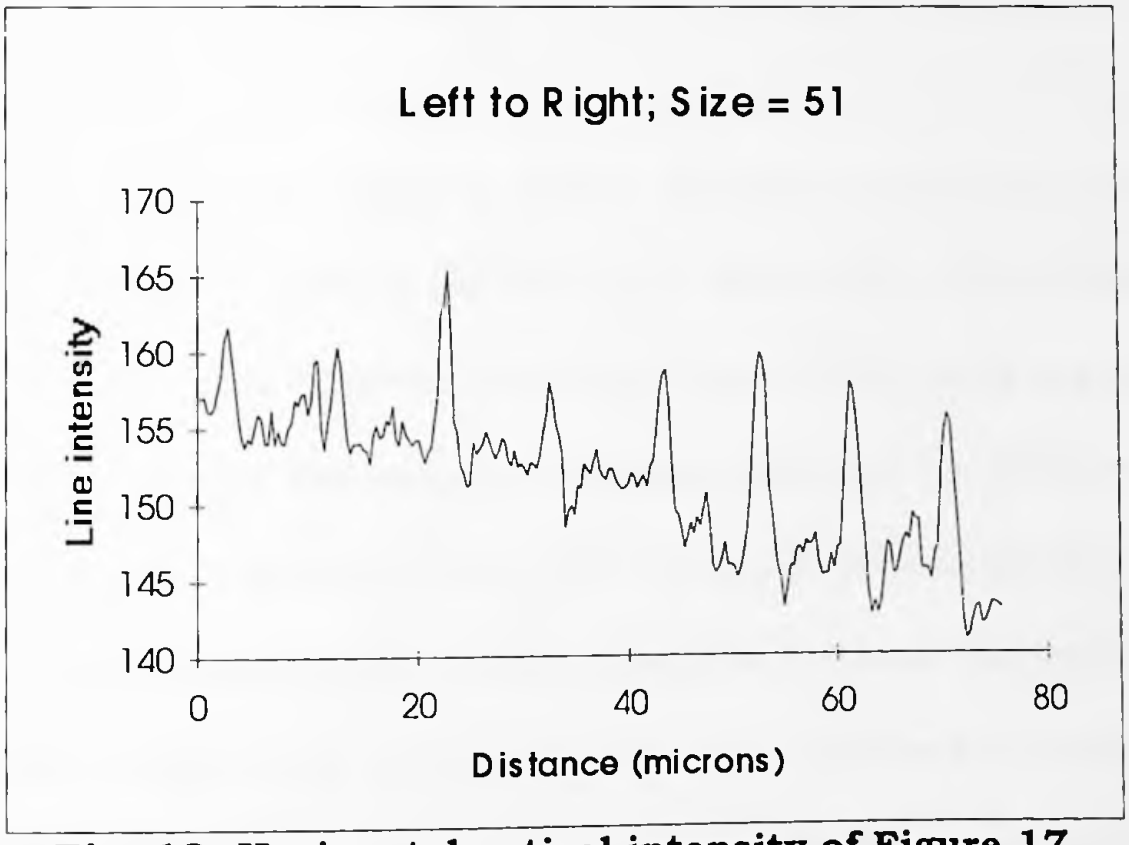

Fig. 19, Horizontal optical intensity of Figure 17.

Notice that in each of the graphs, there is a dip in the intensity on one side of the peaks. This is especially noticeable in

the graph of the vertical intensity (Figure 18). The horizontal intensity graph also shows the same phenomena; however, the shadows (the low points in the graphs) are on the opposite fringe of the red layer. (Note that the vertical graph was taken from the top to the bottom, and the horizontal layer was taken from left to right.) Because of the difference of the location of the shadow, this is believed to be an artifact.

STM Imaging

A crystal from growth #4 was first mounted with silver epoxy, ground, and polished as described earlier. An optical picture of the crystal was taken (Figure 17). Then the crystal and some epoxy was cut out of the ring forming a square about one quarter of an inch on a side. The epoxy and crystal were then subjected to a quick repolishing with 0.03μm grit polish. This was to remove any insulating layer that may have formed because of the length of time it was exposed to air during the optical imaging and the removal of the epoxied crystal from the Bakelite ring. The epoxied crystal was immediately mounted on the STM, and an image was taken (Figure 20).

Even with these steps to reduce the formation of an insulating layer, the STM was able to obtain only a few images before imaging difficulties precluded further imaging. These difficulties are ascribed to the resistivity of the sample becoming too high for STM imaging.

One feature to note in the STM image is the occurrence of what appears to be a ridge at the interfaces between the two layers. The height of the most prominent area was measured by using Sigma Scan to convert the image to gray scale, and then to correlate the intensity of the pixels to the height. This is shown in Figures 20 and 21.

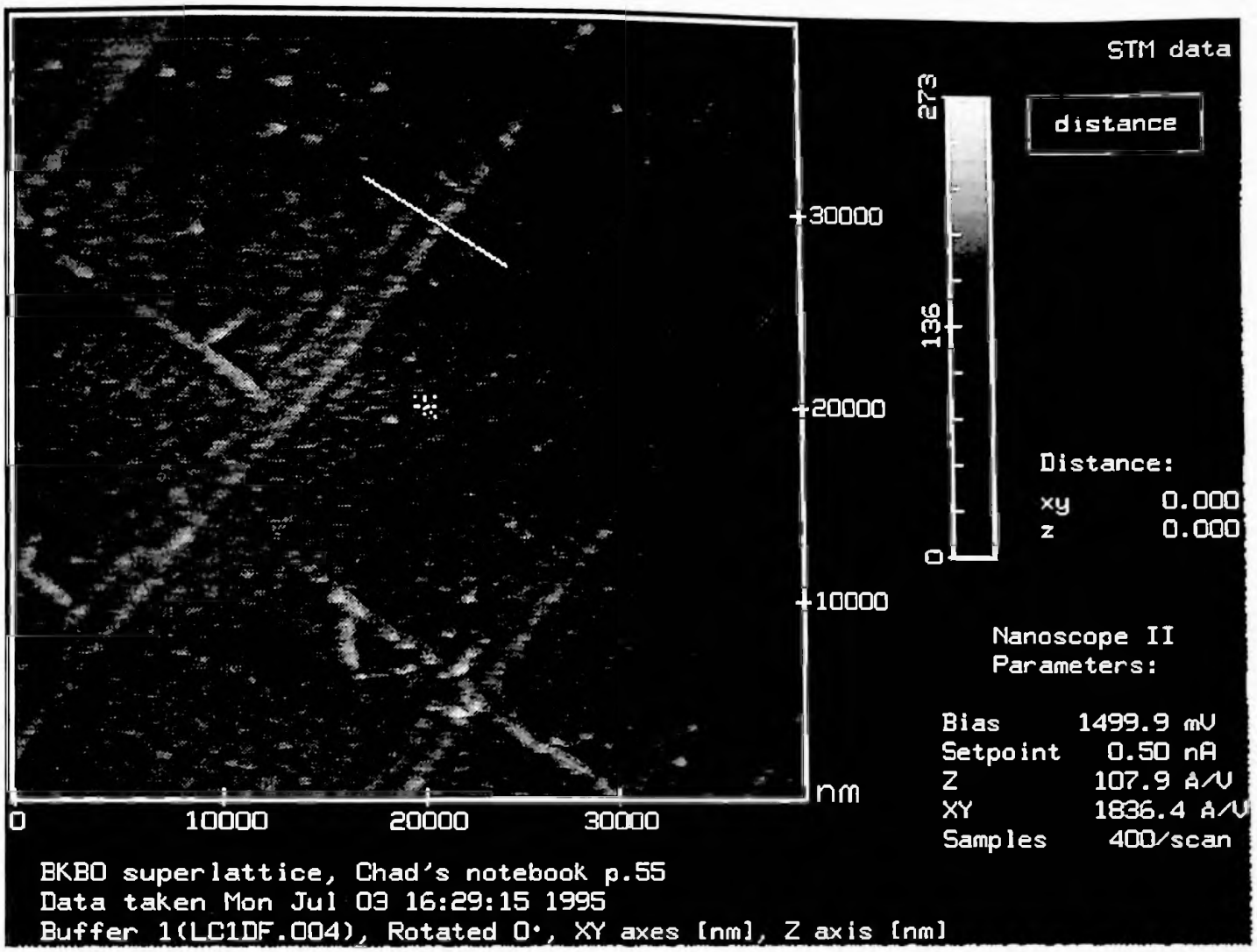

Fig. 20, STM image of layered crystal. The line in the image indicates where the cross section of the ridge was taken for Fig. 21.

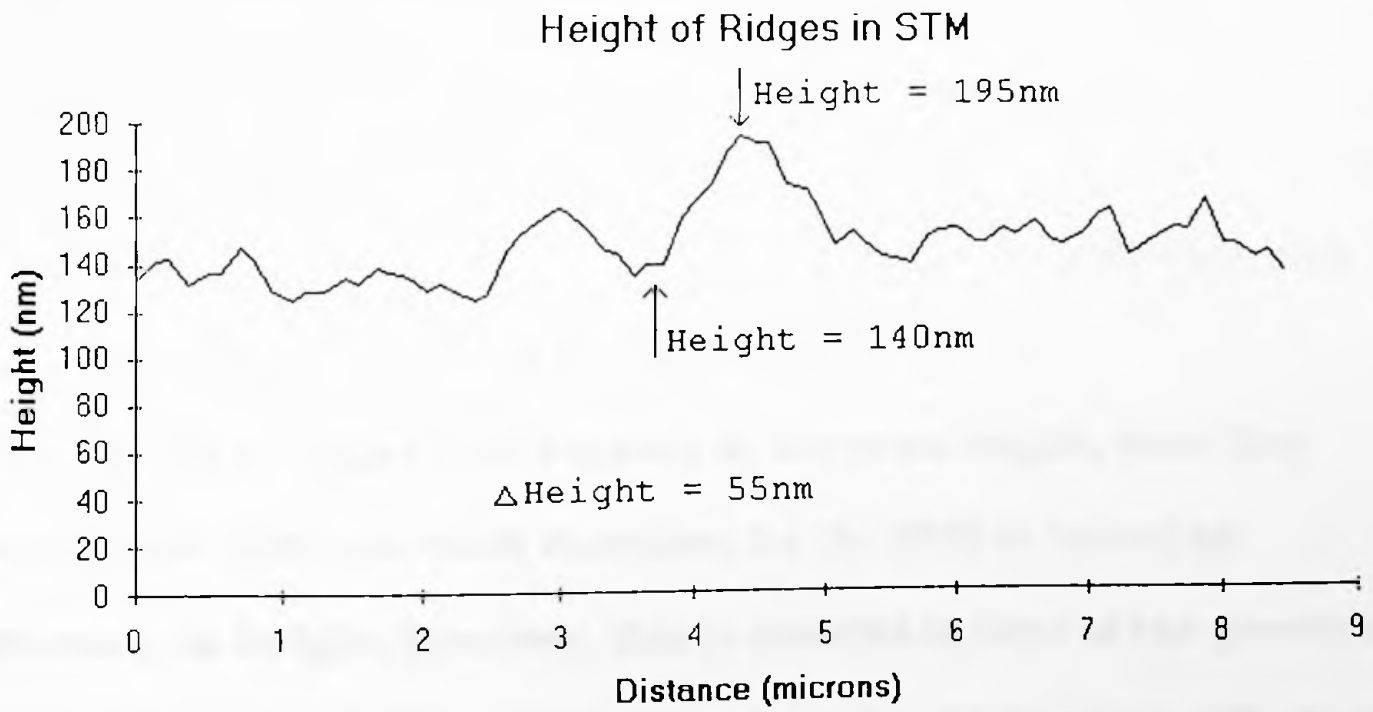

Fig. 21, Cross section of Fig. 20.

This ridge could be due to an actual height difference, or could be due to decreased work function of the sample in this area. A calculation was performed similar to Ming Liang's (29) calculations for the tunneling distance for tungsten (3 Å). She calculated the distance from the tip of the STM to the surface of the substrate using the work function of tungsten using the following equation (30):

$$j = \frac{e^2 V}{4\pi^2 L \delta h} e^{-2L/\delta} \qquad \text{where } \delta = \frac{hc}{\{2mc^2(U-E)\}}$$

In these equations, L is the distance between the tip and the sample surface, and U-E is the work function.

Using her example for tungsten, the distance from the tip to the sample surface was calculated for Se (work function = 5.9) and for Cs (work function = 2.14) (31). These were chosen because they have the highest and lowest work function of the elements.

For Cs, L was found to be 4.03 Å, and for Se, L was found to be 2.78 Å. The difference is only 1.25 Å (0.125 nm) for elements with the largest difference in work functions.

If these ridges were actually at the same height, then they must have different work functions for the STM to record an increase in height. However, this is doubtful in view of the previous calculation which indicates that no known work function difference would cause the STM to indicate a 55 nm difference in height.

An alternative explanation is based on the fact that there is an internal stress due to the epitaxial growth of one composition on top of another. This stress is due to a decreasing lattice parameter as the potassium content increases (32). If the layers are epitaxial, then the interface will be stressed as each layer adjusts to accommodate the lattice parameter of its neighbor. Stress at the interface may be partially relieved at the polished surface by deforming, causing a ridge to appear in the STM image. This same behavior was noted by Switzer *et al.* in his investigation of thallium oxides and thallium lead oxides grown utilizing pulsed potentials (33,34).

Another likely explanation is that corrosion at the interface may be responsible. Chemical reactivity may be enhanced at the interface due to the stress mentioned in the previous paragraph. This would cause a ridge at the interfaces. Although the corrosion material may be insulating, a coating of water may allow for enough conductivity to image the sample.

Comparison of STM and Optical Images

An image obtained by STM was compared to an image obtained by reflectance microscopy. This was done by comparing the size of the layers in each image. A commercial software package called Sigma Scan was used to analyze both images. The distances measured optically were calibrated using a ruled reticle. The STM image placed an internally calibrated rule within the image.

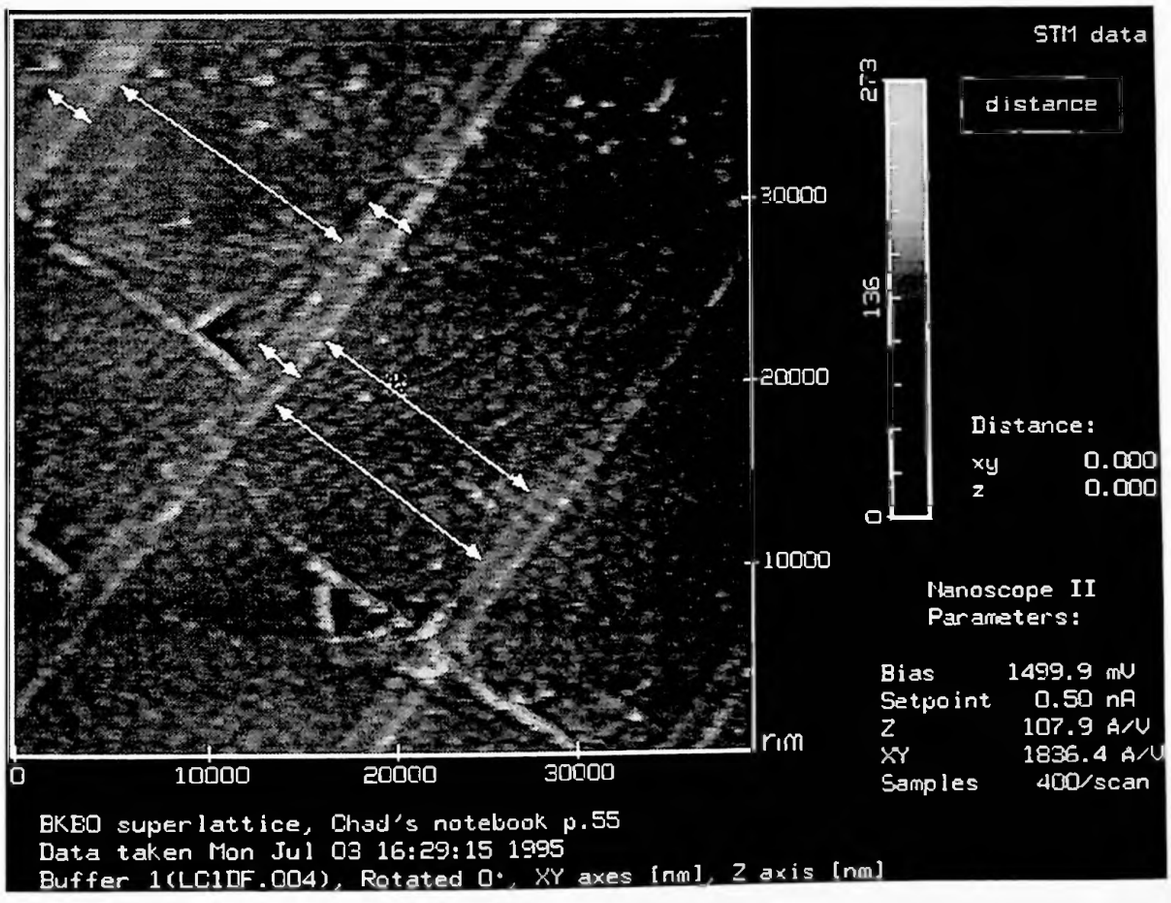

Fig. 22, Gray Scale of STM Image.

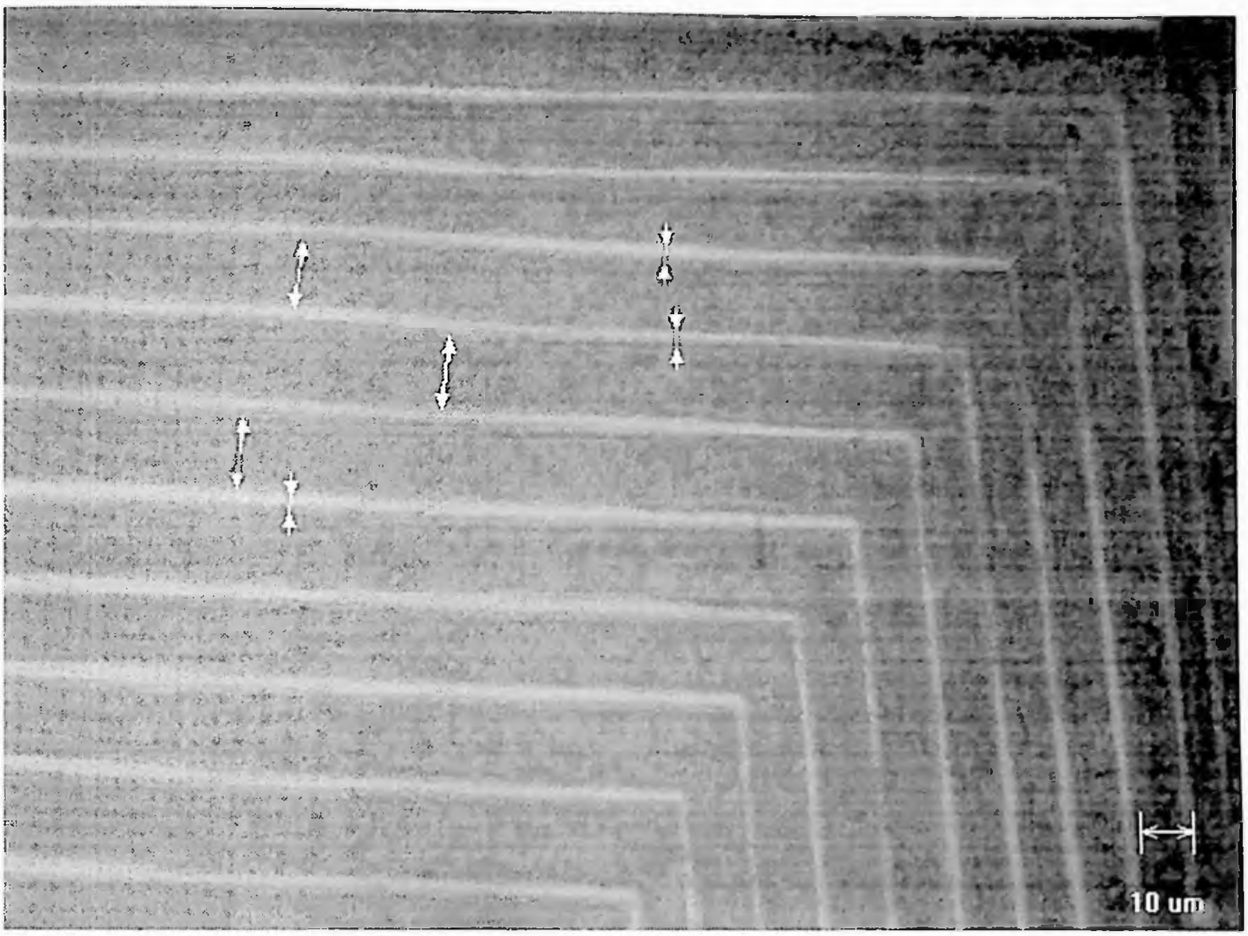

Fig. 23, Gray Scale of Optical Image of crystal imaged by STM.

Measurements were taken in three locations for each layer on both images. The lines of measurement are indicated in the figures as arrows. On the optical image, the red layer was found to have an average width of 2.76*μm*. For the blue layer, the average width was 13.16*μm*. For the STM image, the smaller layer (believed to be red) was 2.67*μm*, and the blue layer was 13.89*μm* (see Table 2).

This comparison demonstrates that the image obtained by the STM was indeed the two different layers, not an artifact produced by

the polishing procedure. The smoothness of the layers and their continuity attest to this as well.

SEM Backscattered Electron Imaging and Etching the Surface of Modulated Crystals

The difficulty in obtaining an STM image was believed to be due to surface contamination. J.M. Rosamilia at AT&T Bell Laboratories reported that single crystals of BKBO were etched with a hot disodium ethylenediaminetetraacete solutions (35). The utility of this etchant for cleaning the surface of our modulated crystals for STM imaging was investigated. However, the surface of the etched crystal became so uneven that even the reflectance microscope was unable to obtain an image due to the small amount of light reflected.

The etched crystal was imaged at the University of Georgia using SEM along with an untreated crystal. Figure 24 is the untreated crystal, and figure 25 is the treated crystal.

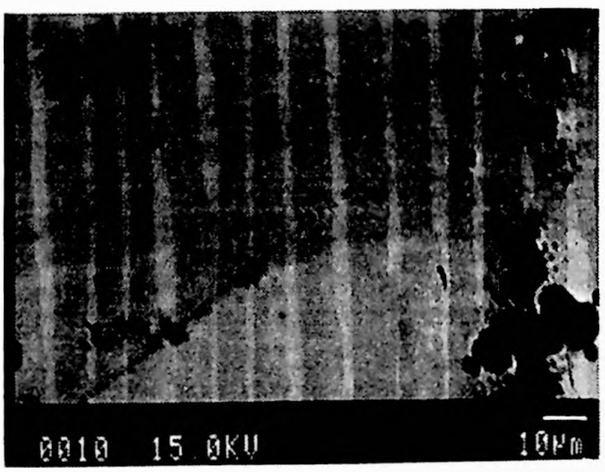

Fig. 24, Backscattered SEM Image of an Untreated Crystal.

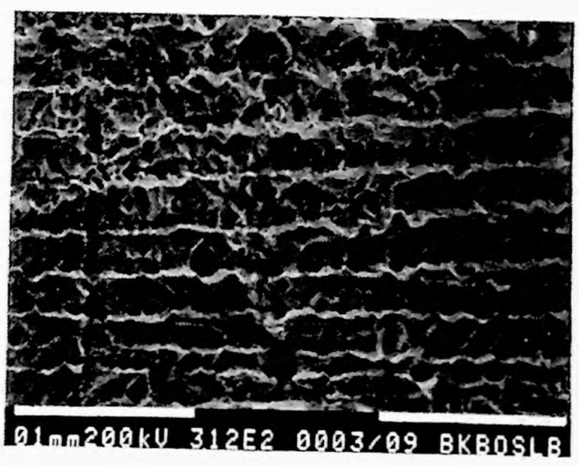

Fig. 25, Backscattered SEM Image of a Treated Crystal. (Scale bar = 0.1 mm)

The backscattered electron image of the untreated crystal reveals the familiar layered structure observed by optical microscopy, and by STM. The crystal that was etched had a surface that was pitted throughout. Although pitting was evident throughout the entire surface, it was not homogeneous. One type of layer appears to be attacked more than the other.

Backscattered SEM was able to distinguish between the two layers in both the treated samples and untreated samples. Even with further refinement it appears that etching with EDTA would prove to be an unsatisfactory method to clean the surface of the crystal in preparation for STM imaging. However, it may be possible to create diffraction gratings using a similar technique.

Growth Rate Measurements

Because the growth is performed under constant potential, the size of the crystals, and ultimately the size of the layers, in general depends upon the amount of time that the potential is applied. The following is a table of layer thicknesses and the amount of time that each potential was applied. The layer thickness was again measured from optical images using Sigmascan. The images of growth #2 and growth #4 had a resolution of ±0.3 microns (the size of each pixel in the images). The images of growth #3 and growth #5 had a resolution of ±0.13 microns (the size of each pixel in the images).

Table 2, Width of Modulated Layers as a Function of Cycle Time

Growth Number and Potential	Time in Seconds	Average length (microns)	Standard Deviation
1) 0.66V 0.68V	2160 576	(6.89) and (6.06)*	(0.72) and (0.69)*
2) 0.66V 0.68V	2160 576	5.52 6.92	0.14 0.56
3) 0.66V 0.68V	2160 2160	3.03 14.40	0.50 0.52
4) 0.66V 0.68V	1800 1800	2.76 13.16	0.16 0.43
5) 0.66V 0.68V	180 72	0.65 0.60	0.054 0.053

* The identity of the layers (0.68V or 0.66V) was undetermined in the BKPBO crystal.

The following are graphical representations of the data presented in the previous table.

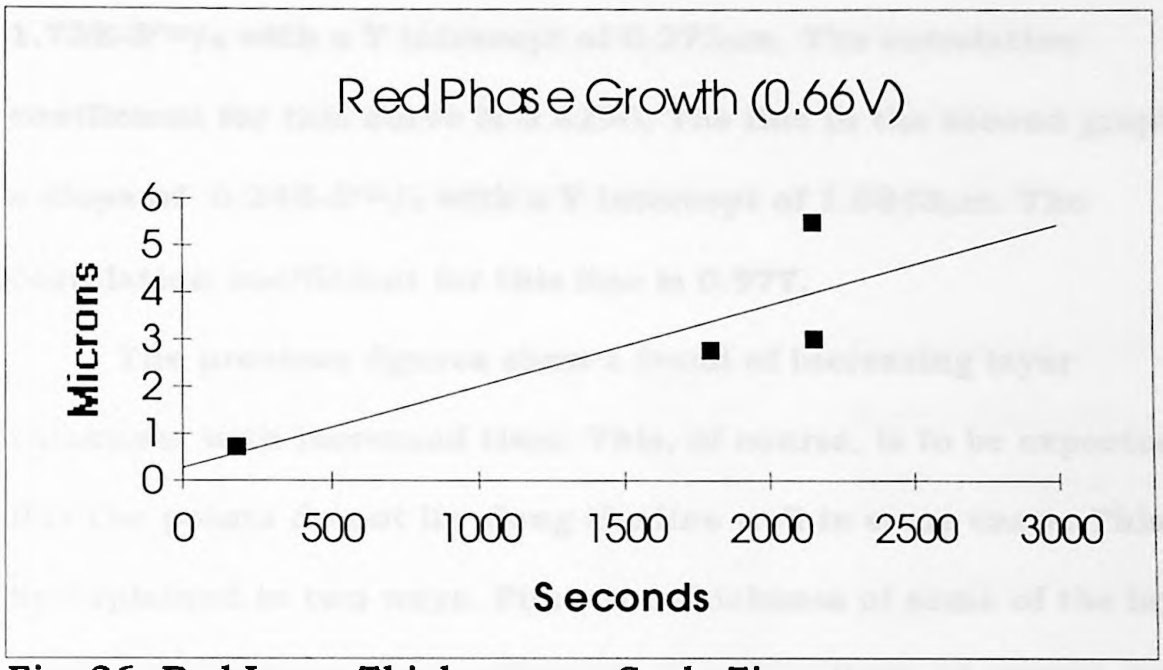

Fig. 26, Red Layer Thickness *vs.* Cycle Time

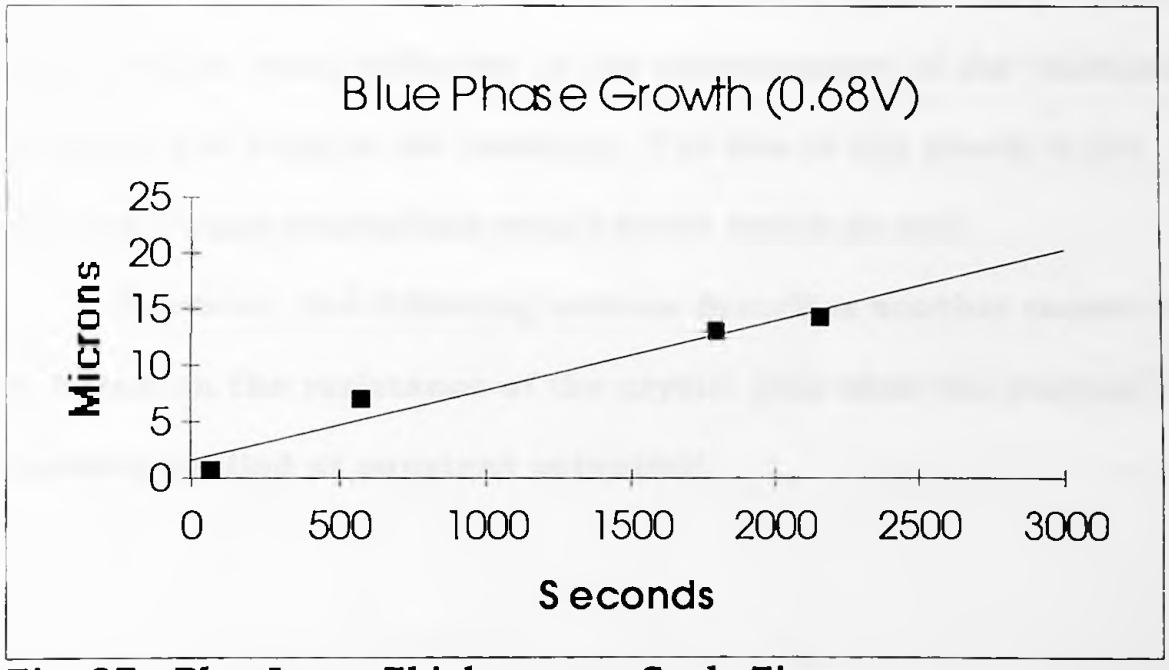

Fig. 27, Blue Layer Thickness *vs.* Cycle Time

The solid line is a linear regression line calculated from the data points. The line in the first graph (0.66V) has a slope of 1.73E-3$^{\mu m}/_{s}$ with a Y intercept of 0.273μm. The correlation coefficient for this curve is 0.8296. The line in the second graph has a slope of 6.24E-3$^{\mu m}/_{s}$ with a Y intercept of 1.5843μm. The correlation coefficient for this line is 0.977.

The previous figures show a trend of increasing layer thickness with increased time. This, of course, is to be expected. But the points do not lie along the line well in some cases. This may be explained in two ways. First, the thickness of some of the layers is coming close to the wavelength of visible light. In growth number five, the layer thickness is within the visible range. This would be expected to cause difficulty in the measurement of the thickness by blurring the edge of the interface. The size of the pixels in the images (image resolution) would cause errors as well.

However, the following section describes another reason which is based on the resistance of the crystal (and thus the amount of current applied at constant potential).

Temporal Dependence of Current

As mentioned on page 13, the crystal growth was monitored by a chart recorder. The following are two representative chart recordings. The first is without modulation (V = 0.68V), and the second began modulation after growing at 0.68V for 3 hours.

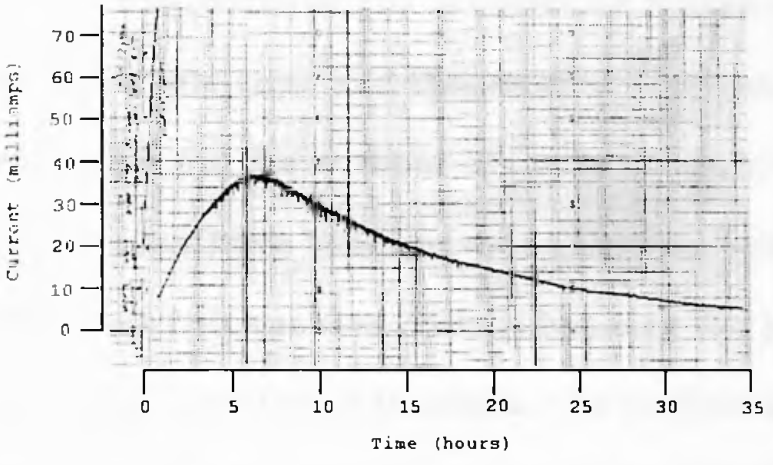

Current Range = 100 mA

Growth time = 35 hours

Maximum current at 6.5 Hours = 36 mA

Chart Speed = 1 cm per hour

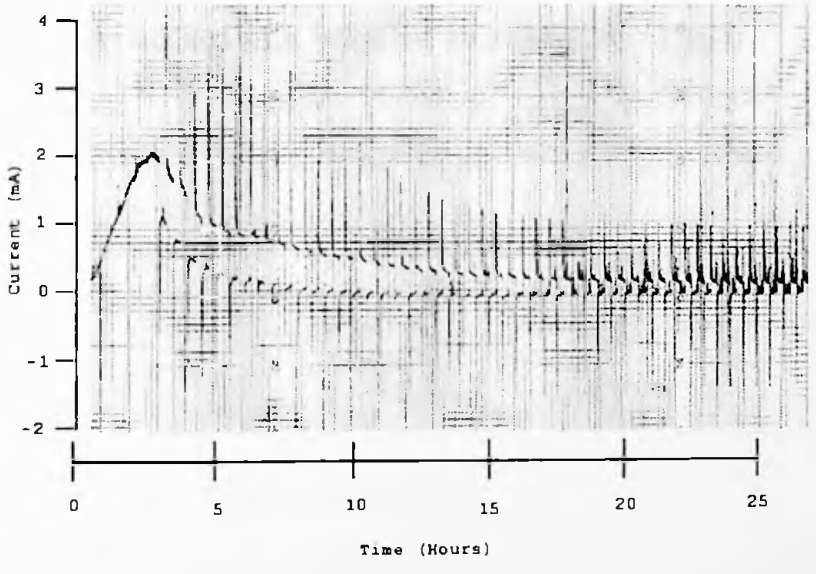

Current Range = 10 mA

Total Growth Time=27hr.

Maximum current at 2.9 hours = 2.1 mA

Current cycling started after 3 hours. 15 minutes at 0.66V and 0.68V.

Chart Speed = 1 cm per hour

Fig. 28, Typical current plots for nonmodulated and modulated growth.

These chart recordings show that the current increases to a maximum, and then decreases at longer times. The initial increase and maximum is perhaps due to increasing surface area as the nucleated crystals grow. The decline is perhaps due to an increase in resistance as the surface of the crystal grows farther from the silver wire electrode.

The width of the modulation within the crystal is dependent on the cycle time and the amount of current density flowing during the cycle (or the number of Coulombs ($A*s/cm^2$)). Even though two layers may have been grown at the same potential, they may have different thicknesses. This is because the previous crystal growth is resistive, and the potential at the surface of the crystal is decreased. Layer thickness would be determined by when the growth occurred on the plot of current *vs.* time.

Current Spikes Accompanying a Potential Transition

During the growth of the crystal the potential is modulated with the square - wave form indicated in Figure 29.

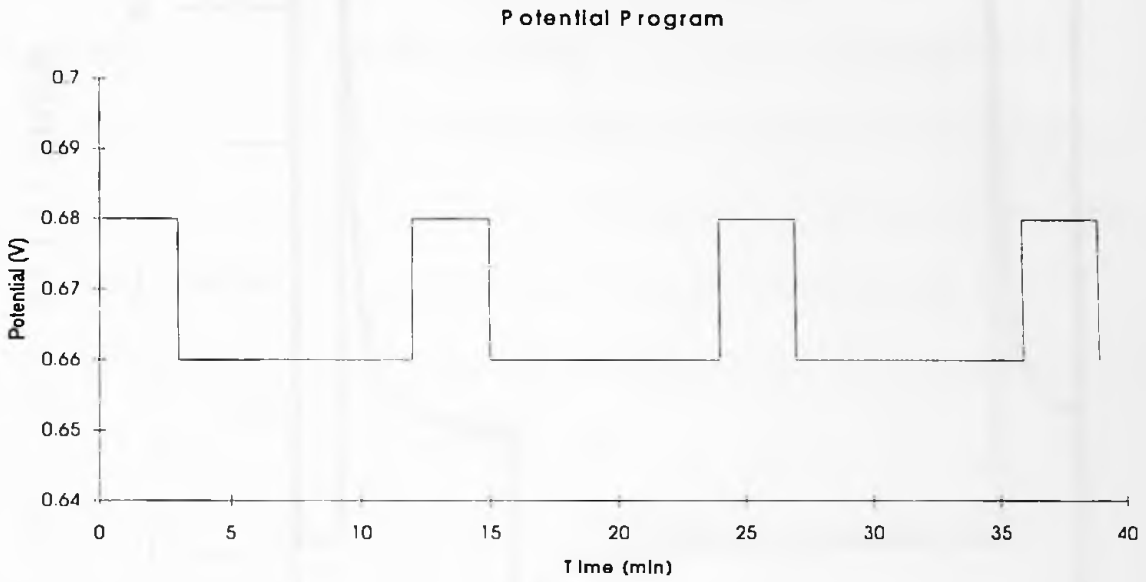

Fig. 29, Potential program. 0.68V for 3 minutes, and 0.66 V for 9 minutes.

Initially, based on Ohm's law (Potential = resistance * current), one might think that a plot of the current should have a square waveform as well. Below is a chart recording of the current for one cycle. To increase clarity, the chart recorder speed had been increased to $1^{cm}/_{min}$. Potentials were 0.66V (for nine minutes), and 0.68V (for three minutes).

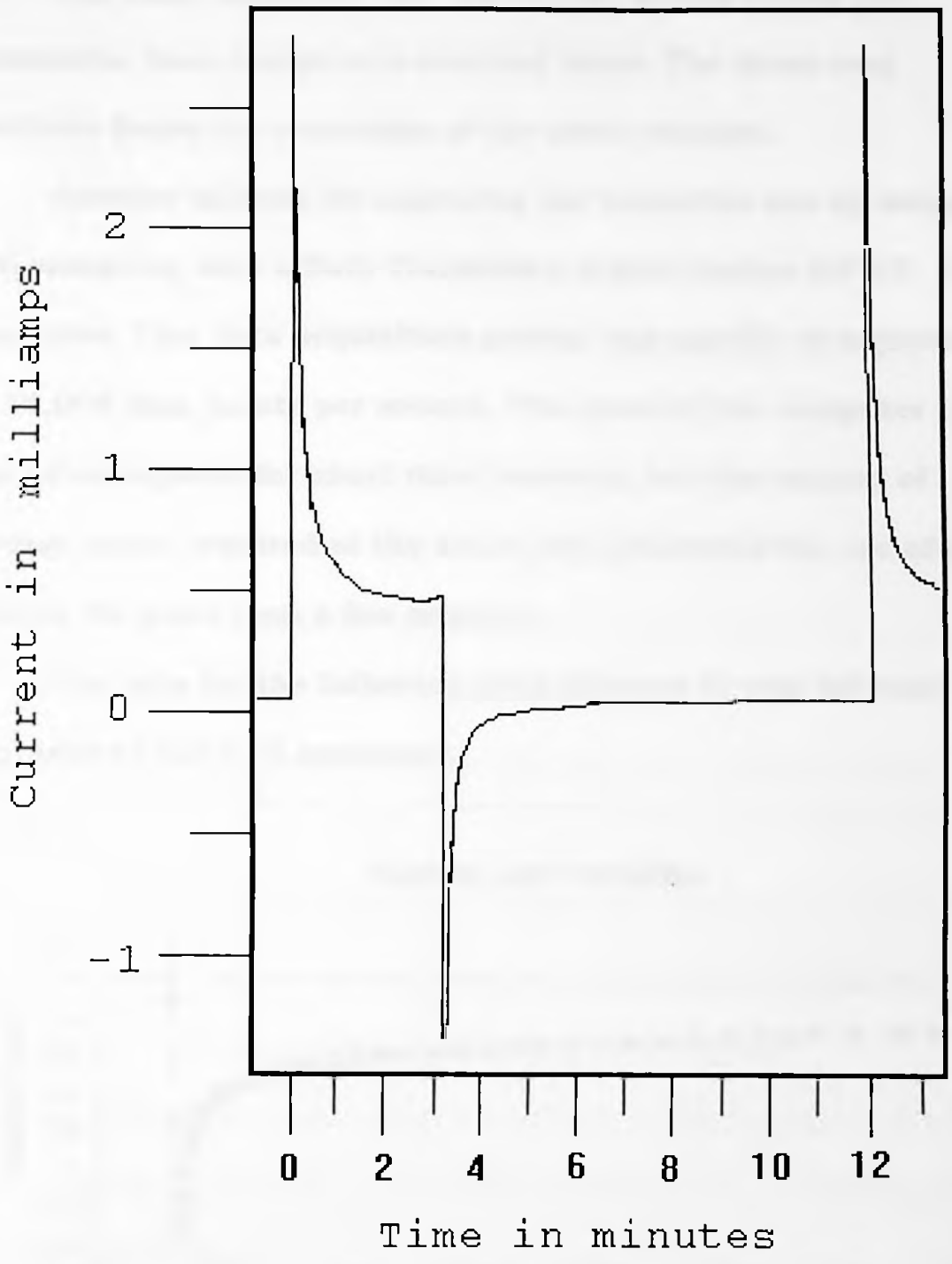

Fig. 30, Plot of current transitions.

The chart indicates that the current spikes during the transients, then decays to a constant value. The decay may continue below the resolution of the chart recorder.

Another method for capturing the transition was by using a 386 computer with a Data Translation model number DT717 A/D converter. This data acquisition system was capable of acquiring up to 15,000 data points per second. The speed of the computer system was advantageous for short time intervals, but the amount of storage space required at the above rate prohibited the use of the system for more than a few minutes.

The data for the following plots (Figures 31 and 32) were captured by the A/D converter.

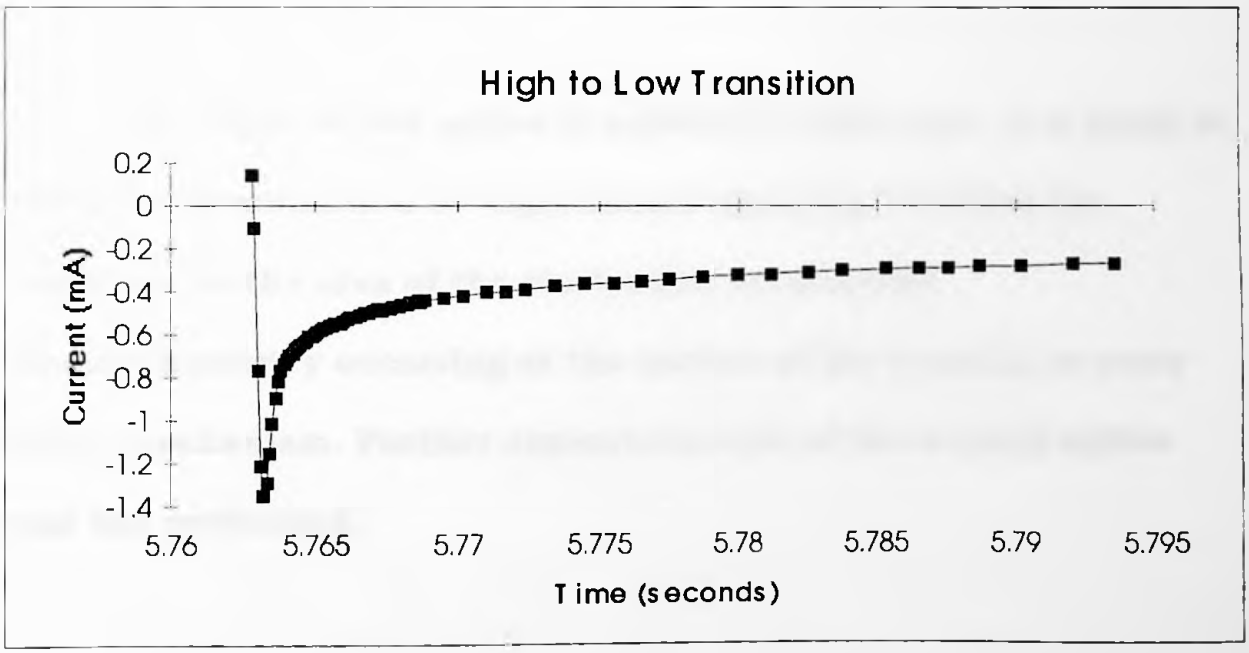

Fig. 31, Current transition accompanying potential switch from 0.68V to 0.66V.

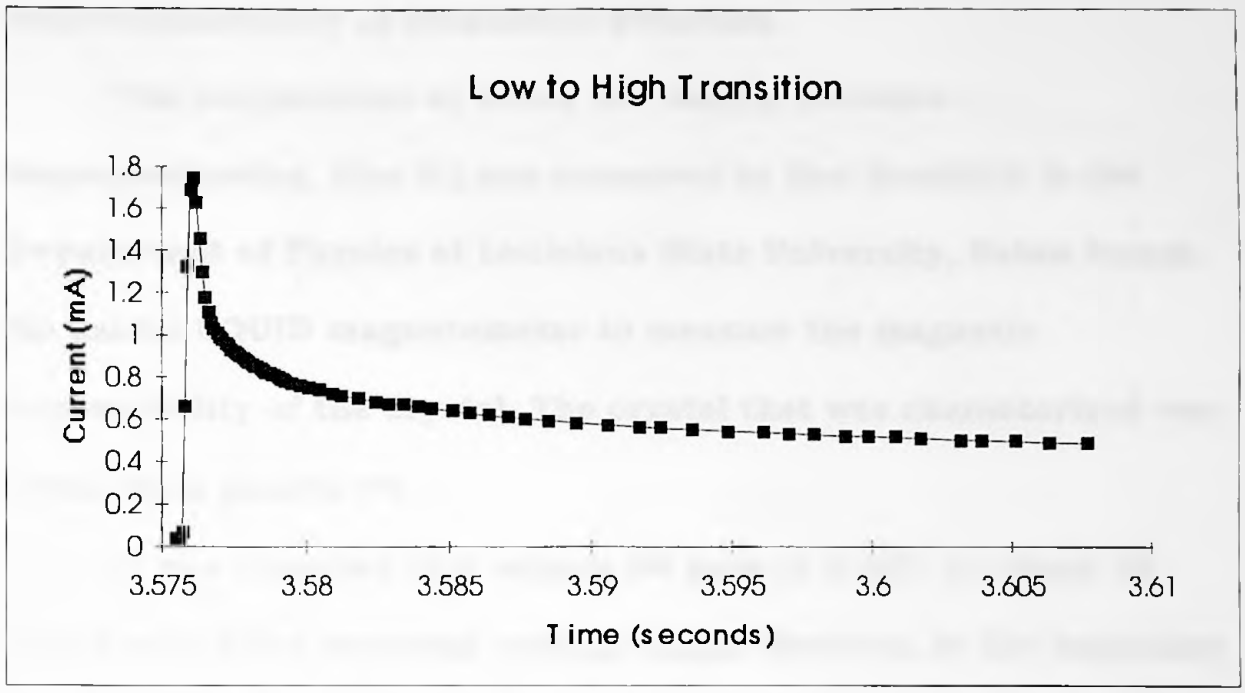

Fig. 32, Current transition accompanying potential switch from 0.66V to 0.68V.

Again the plot shows an initial spike, and then decay as time increases.

The origin of the spikes is unknown at this time. It is likely to involve a combination of capacitance charging, localized ion depletion in the area of the electrodes, unidentified electrochemistry occurring at the surface of the crystals, or some other mechanism. Further characterization of the current spikes was not performed.

Superconductivity of Modulated Structure

The temperature at which the sample becomes superconducting (the T_c) was measured by Roy Goodrich in the Department of Physics at Louisiana State University, Baton Rouge. He used a SQUID magnetometer to measure the magnetic susceptibility of the crystal. The crystal that was characterized was taken from growth #4.

It was intended that sample #4 grow at 0.68V for about 24 hours before the potential cycling began. However, at the beginning of the cycle, the "base" crystals fell off the electrode. The result of this was that all crystals grown were multilayered throughout the crystal. Thus, the multilayers are superconducting, and not just a 0.68V core. The following graph summarizes susceptibility as a function of temperature.

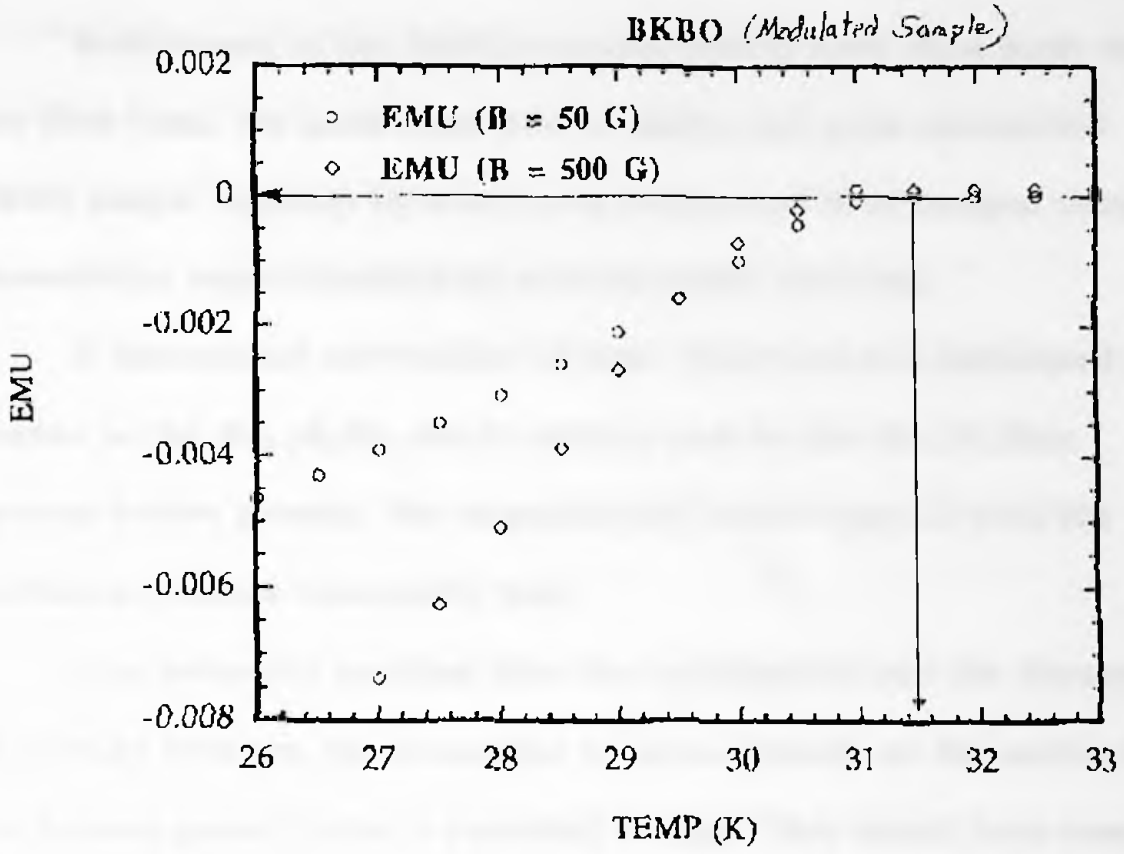

Fig. 33, Magnetic susceptibility of growth #4 *vs.* Temperature Nominal size 2.76μ for insulating layer (0.66V) and 13.6μ for the superconducting layer (0.68V) (30 minutes each).

Reading from right to left (higher temperature to lower temperature) the curve begins to decrease at approximately 31.4 K . This is near the reported value for BKBO (36).

The plot does show that the superconducting temperature is not affected by multilayering of the crystal on this size scale. A smaller layering wavelength in the crystal may yield observable effects.

Conclusion

Multilayers of the BKBO superconductor have been made for the first time. We have been able to design and grow modulated BKBO single crystals by electrodeposition and have imaged them. Modulation was controlled by potentiostatic methods.

A theoretical calculation of layer thickness was performed for oxides in the $Ba_{1-y}K_yBi_{1-x}Pb_xO_3$ system and for the $Ba_{1-x}K_xBiO_3$ system before growth. The experimental results agreed with the calculated values reasonably well.

One potential problem that was anticipated was the disruption of epitaxy through the formation of microcrystals on the surface of the former growth after a potential change. This would have resulted in the formation and growth of polycrystalline layers, making the transition between the layers jagged and uneven. However, this was not observed. Transitions between the layers were distinct and smooth.

Under the optical microscope, the transitions between the layers appear to be relatively defect free. The interfaces are well defined, straight and parallel to the 100 direction. The same is true when the crystals are observed using SEM. Under STM, again the layers appear smooth with a distinct transition.

The smoothness of the interfaces indicates that the change in potential does not adversely affect the growth of the crystals. Judging by the lack of twinning or polycrystallinity, the layers appear to grow epitaxial with respect to each other.

EDTA was used as an etchant. The etchant differentially attacked the layers in the sample. This was imaged by backscattered SEM.

Although there is only a small compositional difference in the two layers of the multilayered crystals, backscattered SEM was able to distinguish between the layers in both etched samples, and unetched samples.

A clear relationship between deposition time and layer thickness was determined. This makes the calculation of layer thickness, and therefore the design of multilayer materials, possible before initiating crystal growth.

The deposition current spikes during the potential transition. Features observed using STM appear to be correlated with the transients. The origin of this phenomenon was left undetermined.

The transition temperature (T_c) observed for a multilayered sample appears similar to the literature values for bulk material. This indicates that T_c is not affected by the layering of the crystal at this size scale.

References

(1) *The Science and Technology of Superconductivity* Gregory, W.D.; Mathews, W.N.; Edelsack, E.A. Eds., Plenum Press, 1973, vol1, p7.

(2) *Handbook of Chemistry and Physics* Lide, D.R. Ed. 72nd ed. :CRC Press, Inc Boca Raton, Florida, p12-41.

(3) Koperdraad, R.; Thesis, Vrije Universitet te Amsterdam, 1995, p5.

(4) Koperdraad, R.; Thesis, Vrije Universitet te Amsterdam, 1995, p10.

(5) Koperdraad, R.; Thesis, Vrije Universitet te Amsterdam, 1995, p10.

(6) Wu, M.K.; Ahsburn, J.R.; Torng, C.J.; Hor, P.H.; Meng, R.L.; Gao, L.; Huang, Z.J.; Wang, Y.Q.; Chu, C.W. *Physical Review Letters* 1987, 58, 908.

(7) Brongersma, S.; Thesis, Vrije Universitet te Amsterdam, 1996, p2.

(8) Sleight, A. W.; Gilson, J. L.; Bierstedt, P. E. *Solid State Commun.* 1975, 7, 27.

(9) Szabo, P.; Samuely, P.; Bobrov, L.N.; Marcus, J.; Escribe-Filippini, C.; Affronte, M. *Physica C* 1994, 235-240, 1873.

(10) Wei, J.; Degani, M.H.; Kalia, R.K.; Vashishta, P. *Physical Review B* 1992, 45, 5535.

(11) Gao, F.; Whitaker, J.F.; Liu, Y.; Uher, C.; Platt, C.E.; Klein, M.V. *Physical Review B*, 1995, 52, 3607.

(12) Brongersma, S.; Thesis, Vrije Universitet te Amsterdam, 1996, p3.

(13) Strongin, M.; Kammerer, O.F.; Crow, J.E.; Parks, R.D.; Douglass Jr., D.H.; Jensen, M.A. *Physical Review Letters*, 1968, 21, 1320.

(14) *The Science and Technology of Superconductivity* Gregory, W.D.; Mathews, W.N.; Edelsack, E.A. Eds., Plenum Press, 1973, p23.

(15) Brongersma, S.; Thesis, Vrije Universitet te Amsterdam, 1996, p2.

(16) Hellman, E. S.; Hartford, Jr., E. H. *Physical Review B* 1995, 52, 6822.

(17) Pei, S.; Jorgensen, J.D.; Dabrowski, B.; Hinks, D.G.; Richards, D.R.; Mitchell, A.W.; Newsam, J.M.; Sinha, S.K.; Vaknin, D.; Jacobson, A.J. *Physical Review B* 1990, 41, 4126.

(18) Wei, J.; Degani, M.H.; Kalia, R.K.; Vashishta, P. *Physical Review B* 1992, 45, 5535.

(19) Norton, M.L. *Materials Research Bulletin*, 1989, 24, 1391.

(20) Norton, M.L.; Tang, H. *Chemistry of Materials*, 1991, 3, 431.

(21) Han, P.D.; Chang, L.; Payne, D.A. *ICCG-10* August 16-22, 1992.

(22) Han, P.D.; Chang, L.; Payne, D.A. *ICCG-10* August 16-22, 1992.

(23) Zhuang, B.; Thesis, Marshall University 1993.

(24) Zhuang, B.; Thesis, Marshall University 1993, p52.

(25) Marx, D. T.; Randaelli, P. G.; Jorgensen, J. D.; Hitterman, R. L.; Hinks, D.G.; Pei, S.; Dabrowski, B. *Physical Review B*, 1992, 46, 1144.

(26) Zhuang, B.; Thesis, Marshall University 1993, p33.

(27) Zhuang, B.; Thesis, Marshall University 1993, p52.

(28) Han, P.D.; Chang, L.; Payne, D.A. *ICCG-10* August 16-22, 1992.

(29) Liang, M.; Thesis, Marshall University 1995.

(30) Scrway, R. A.; Moses, C. J. ; Moyer, C. A. *Modern Physics*; Saunders College Publishing: New York, 1989.

(31) *Handbook of Chemistry and Physics* Weast, R. C. Ed. 61st ed. CRC Press, Inc Boca Raton, Florida, pE-83.

(32) Pei, S.; Jorgensen, J.D.; Dabrowski, B.; Hinks, D.G.; Richards, D.R.; Mitchell, A.W.; Newsam, J.M.; Sinha, S.K.; Vaknin, D.; Jacobson, A.J. *Physical Review B* 1990, 41, 4126.

(33) Switzer, J.A.; Raffaelle, R.P.; Phillips, R.J.; Hung, C.; Golden, T.D. *Science*, 1992, 258, 1918.

(34) Switzer, J.A.; Hung, C.; Breyfogle, B.E.; Shumsky, M.G.; Leeuwen, R.V.; Golden T.D. *Science*, 1994, 264, 1573.

(35) Rosamilia, J.M.; Glarum, S.H.; Cava, R.J.; Batlogg, B.; Miller, B. *Physica C*, 1991, 182, 285.

(36) Cava, R.J.; Siegrist, T.; Peck Jr., W.F.; Krajewski, J.J.; Batlogg, B.; Rosamilia, J. *Physical Review B*, 1991, 44, 9746.

VITA

Chad Huffman was born in Beckley, West Virginia. He spent most of his childhood in Ona, West Virginia. He received his Bachelor of Science in Chemistry from Marshall University in 1992. He has accepted a teaching assistantship at Rice University for the fall of 1996 where he will work toward the Ph.D. degree in Chemistry, specifically in the area of Nanotechnology.